

# Elevating Growth Factor Responsiveness and Axon Regeneration by Modulating Presynaptic Inputs

## Highlights

- Lin28 overexpression potentiates IGF1-mediated regeneration of injured RGC axons
- Lin28 effects on IGF1-mediated axon regeneration act via amacrine cells
- RGC injury hyperactivates amacrine; silencing them allows IGF1 signaling
- RGC primary cilia concentrated IGF1R is lost after injury and reduces IGF1 potency

## Authors

Yiling Zhang, Philip R. Williams, Anne Jacobi, ..., Nicholas C. Brecha, Daniel Kerschensteiner, Zhigang He

## Correspondence

prwillia@wustl.edu

## In Brief

Zhang et al. (2019) find that amacrine cell hyperactivation after RGC axotomy prevents IGF1 responsiveness. Blocking amacrine cell synaptic activity potentiates IGF1-mediated axon regeneration by maintaining IGF1R localization to primary cilia, a localization that is normally lost in injured RGCs.

# Elevating Growth Factor Responsiveness and Axon Regeneration by Modulating Presynaptic Inputs

Yiling Zhang,<sup>1,5</sup> Philip R. Williams,<sup>1,2,5,6,\*</sup> Anne Jacobi,<sup>1</sup> Chen Wang,<sup>1</sup> Anurag Goel,<sup>2</sup> Arlene A. Hirano,<sup>3,4</sup> Nicholas C. Brecha,<sup>3,4</sup> Daniel Kerschensteiner,<sup>2</sup> and Zhigang He<sup>1</sup>

<sup>1</sup>F.M. Kirby Neurobiology Center, Children's Hospital, and Department of Neurology, Harvard Medical School, Boston, MA, USA

<sup>2</sup>Department of Ophthalmology and Visual Sciences, Washington University School of Medicine, St. Louis, MO, USA

<sup>3</sup>Department of Neurobiology, David Geffen School of Medicine at UCLA, Los Angeles, CA 90095, USA

<sup>4</sup>United States Veterans Administration Greater Los Angeles Healthcare System, Los Angeles, CA, USA

<sup>5</sup>These authors contributed equally

<sup>6</sup>Lead Contact

\*Correspondence: [prwillia@wustl.edu](mailto:prwillia@wustl.edu)

<https://doi.org/10.1016/j.neuron.2019.04.033>

## SUMMARY

Despite robust effects on immature neurons, growth factors minimally promote axon regeneration in the adult central nervous system (CNS). Attempting to improve growth-factor responsiveness in mature neurons by dedifferentiation, we overexpressed Lin28 in the retina. Lin28-treated retinas responded to insulin-like growth factor-1 (IGF1) by initiating retinal ganglion cell (RGC) axon regeneration after axotomy. Surprisingly, this effect was cell non-autonomous. Lin28 expression was required only in amacrine cells, inhibitory neurons that innervate RGCs. Ultimately, we found that optic-nerve crush pathologically upregulated activity in amacrine cells, which reduced RGC electrical activity and suppressed growth-factor signaling. Silencing amacrine cells or pharmacologically blocking inhibitory neurotransmission also induced IGF1 competence. Remarkably, RGCs regenerating across these manipulations localized IGF1 receptor to their primary cilia, which maintained their signaling competence and regenerative ability. Thus, our results reveal a circuit-based mechanism that regulates CNS axon regeneration and implicate primary cilia as a regenerative signaling hub.

## INTRODUCTION

Since cellular growth is essential for regeneration, external growth-promoting factors in the local environment provide the primary driving force for regeneration. Thus, the availability of growth factors and the cellular responsiveness to these factors are critical for dictating the regenerative ability of a cell or tissue. Attempts to regenerate damaged and diseased axons using neurotrophic growth factors have been primarily unsuccessful (Thoenen and Sendtner, 2002). An underlying confound for growth-factor application is that, in contrast to immature

neurons, mature neurons are regeneration incompetent and often exhibit decreased responsiveness to growth factors (Duan et al., 2015; Goldberg et al., 2002), which is even further diminished by injury (Belin et al., 2015; Shen et al., 1999). In principle, any step along the course of signal initiation and transduction (e.g., receptor availability, signal propagation, or silencing inhibitory pathways) could be targeted to improve neuronal responsiveness to growth factors. In this regard, activation of the downstream effector of multiple growth factor cascades PI3K/mTOR, by deletion of its negative regulator PTEN, in adult cortical neurons and RGCs is able to promote robust axon regeneration after injury, even in the absence of growth factors (Liu et al., 2010; Park et al., 2008; Zukor et al., 2013).

Intriguingly, reduced responsiveness to extracellular factors appears to be a common feature for aging cells and in extreme cases of metabolic dysfunction like type 2 diabetes, in which the cells in aging organisms lose insulin-signaling capacity (Goldstein, 2002). Recent studies demonstrated that, in mice, overexpression of Lin28, a heterochronic gene initially identified in *C. elegans* (Ambros, 1989; Ambros and Horvitz, 1984), promotes an insulin-sensitized state that resists high-fat-diet-induced diabetes and removes let-7-mediated inhibition of insulin and insulin-like growth-factor receptor (IGFR) family expression (Zhu et al., 2011), suggesting an avenue for manipulating cellular responses to extracellular factors. Additionally, Lin28 on its own has been shown to regrow various tissues, including skin, hair, and digits (Shyh-Chang et al., 2013), along with modest regeneration of RGC axons after optic nerve crush (Wang et al., 2018).

Herein, we demonstrate that Lin28 overexpression in the retina increases RGC survival and allows RGCs to respond to growth factors by mounting a regenerative response following optic nerve crush. Interestingly, this effect was not cell intrinsic, as Lin28 was required in amacrine cells and not RGCs. Indeed, examining the amacrine cell response to optic nerve crush, we found that amacrine cells become hyperactivated following RGC injury. Reducing amacrine cell presynaptic inhibition of RGCs, either virally or pharmacologically, similarly promoted RGC survival and growth-factor responsiveness. Notably, we discovered that the primary cilia were a point of convergence

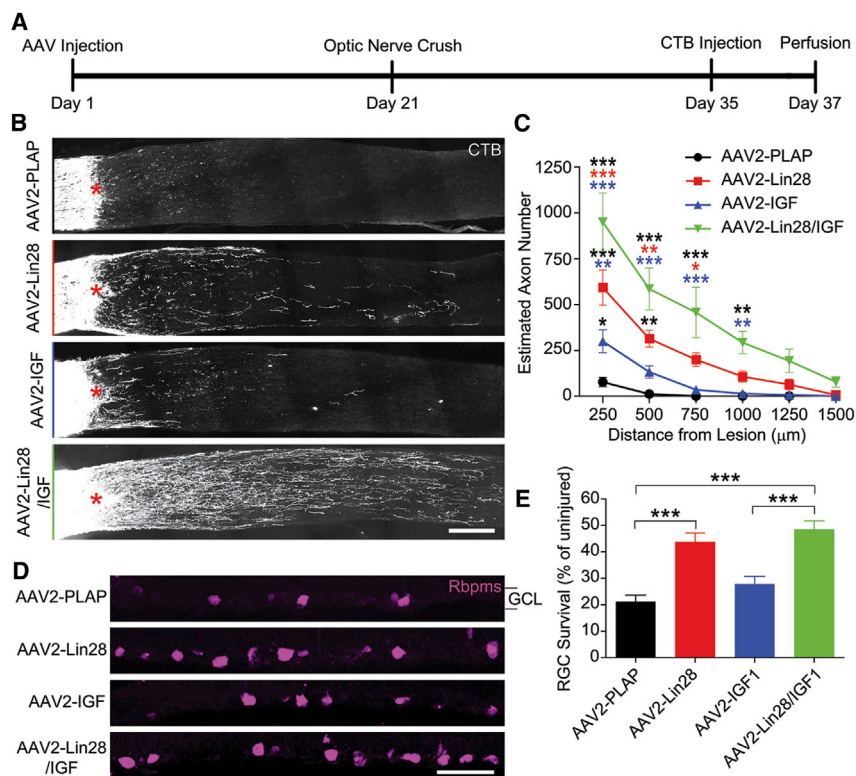


**Figure 1. Combinatorial Treatment with Lin28 and IGF1 Induces Robust Axon Regeneration**

(A) Time course of optic nerve crush and regeneration experiments.

(B) Representative confocal image stacks of optic nerve cryosections showing regenerated RGC axons labeled by CTB intraocular injection 2 weeks after crush in control and treatment conditions. Crush site indicated by red asterisk.

(C) Quantification of the extent of RGC axon regeneration in treatment groups. Asterisk colors indicate the group that the p value was significant against (i.e., black tested against AAV2-PLAP, red tested against AAV2-Lin28).

(D) Representative confocal image stacks of retinal cross-sections stained with the RGC marker Rbpm.

(E) Quantification of RGC survival in treatment groups relative to RGC density observed in intact retinas. n = 5–6 mice per group.

Scale bar, 200 and 50 μm in (B) and (D), respectively. \*, \*\*, \*\*\*p < 0.05, 0.01, 0.001, respectively. See also Figure S1.

for amacrine-cell-silencing-mediated RGC regeneration. In RGCs, IGF1R expression is concentrated in primary cilia; this localization is lost after optic nerve crush. Amacrine cell manipulations maintain IGF1R expression in primary cilia of regenerating RGCs, and removing primary cilia reduced regeneration of treated RGCs. Together, our data show that growth-factor signaling after cell damage can be negatively regulated by presynaptic neurons.

## RESULTS

### Lin28 Potentiates Growth-Factor Responsiveness in Injured RGCs

To determine whether Lin28 could promote responsiveness to growth factors, we tested whether AAV2-mediated expression of Lin28, in combination with AAV2-IGF1, AAV2-BDNF, or AAV2-NT-3, could potentiate regeneration of RGCs after an optic nerve crush in adult mice. Three weeks after intravitreal virus injection of singular treatments, combination treatments, or AAV2-PLAP (placental alkaline phosphatase) as a control (Park et al., 2008), the optic nerve was crushed and, after another 2 weeks, axon regeneration was monitored by intraocular injection of the anterograde axonal tracer Alexa Fluor 555-conjugated cholera toxin subunit B (CTB) (Figure 1A). While mice injected with AAV2-Lin28, AAV2-IGF1, or AAV2-BDNF demonstrated mild RGC regeneration as previously described (Duan et al., 2015; Wang et al., 2018), the combination of Lin28 and IGF1 or BDNF led to robust axon regeneration beyond that seen with any singular treatment (Figures 1B, 1C, S1A, and S1B). Lin28 expression in the retina did not potentiate

the minimal effects of AAV2-NT-3 delivery (Figures S1C and S1D). Additionally, Lin28 treatment, either alone or in combination with IGF1, significantly reduced the RGC death that normally follows axotomy in that survival roughly doubled relative to PLAP-treated controls at 2 weeks after injury, while AAV2-IGF1 treatment alone had no survival-promoting effects (Figures 1D and 1E). Since axon regeneration was better potentiated in combination with IGF1, our subsequent experiments focused on IGF1 and not BDNF or NT-3.

### Lin28-Mediated RGC Survival and IGF1-Dependent Regeneration Are Not Cell Intrinsic

Lin28 is not expressed in mature retina (not shown), and intravitreal injection of AAV2-CAG-Lin28 resulted in transgene expression, visualized by immunostaining with antibodies against Lin28, in RGCs as well as two populations of upstream primarily inhibitory interneurons, amacrine and horizontal cells (Figures 2A, 2B, and S2). To determine whether IGF1 signaling potentiation by Lin28 was cell intrinsic, we restricted its expression to RGCs using Vglut2-Cre transgenic mice (Ellis et al., 2016). We expressed Lin28 only in RGCs by co-injecting AAV2-FLEX-Lin28 into the vitreous bodies of Vglut2-Cre transgenic mice (Figures 2C and 2D). Surprisingly, while selective expression of Lin28 in RGCs alone recapitulated the modest regenerative effects seen with non-restricted expression, the combination of RGC-specific Lin28 expression and widespread IGF1 showed no further increase in regeneration (Figures 2E and 2F). Importantly, such a result indicates that the effects of Lin28 and IGF1 observed with broad overexpression (Figures 1B and 1C) are not likely additive, as both individual responses could be observed in Vglut2-Cre mice. Furthermore, AAV2-FLEX-Lin28 into Vglut2-Cre mice also failed to promote RGC survival (Figure 2G).

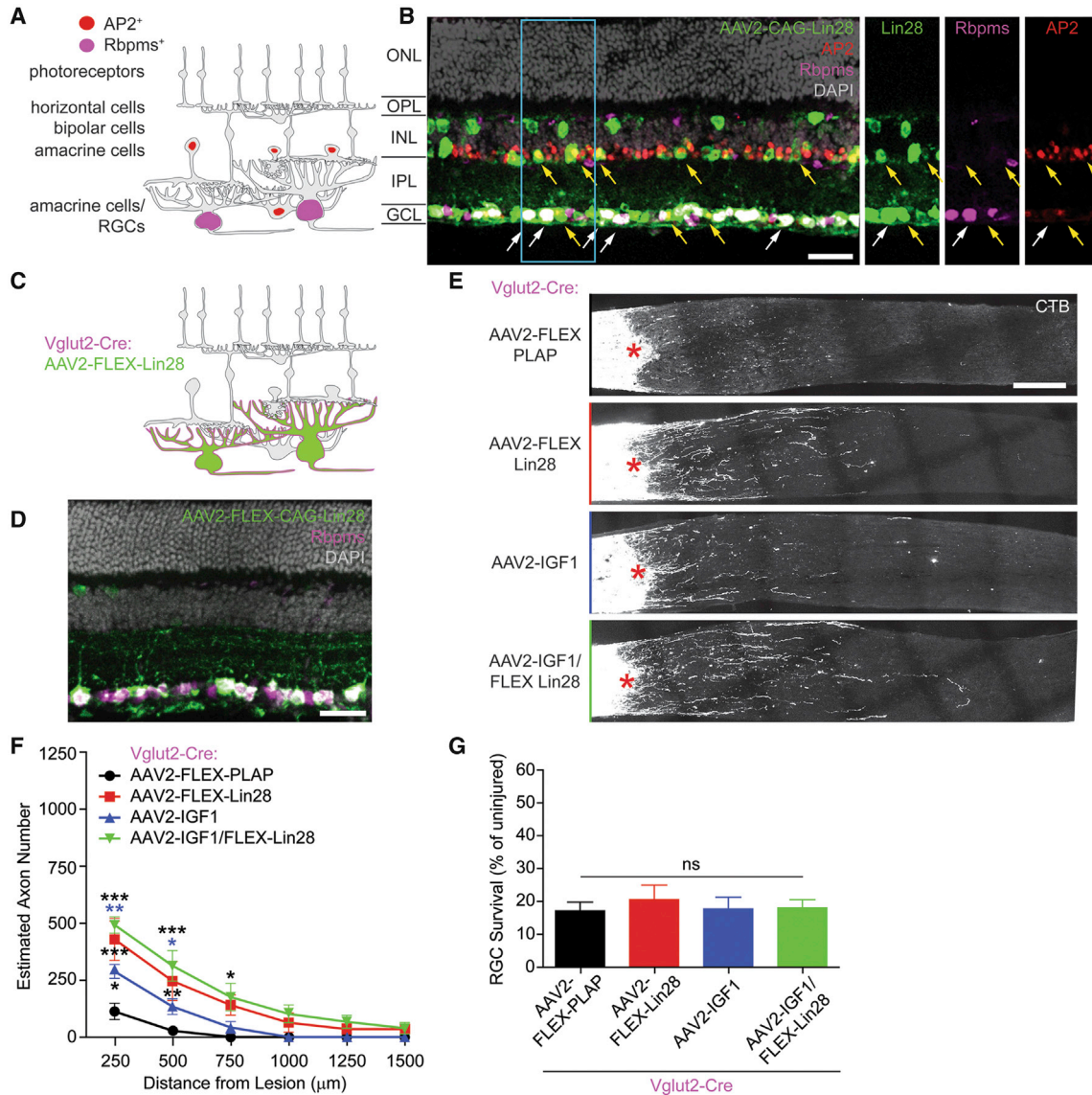


**Figure 2. Lin28-Mediated Axon Regeneration Is Not Intrinsic**

(A and B) Schematic (A) and example (B) confocal image stack demonstrating expression of AAV2-Lin28 in RGCs, amacrine cells, and horizontal cells in the intact retina. White arrows indicate Rbpms- (magenta-) labeled RGCs that express Lin28 (green), while yellow arrows indicated AP2- (red-) labeled amacrine cells that express Lin28. Horizontal cell expression was inferred by location and morphology of AP2 negative cells. ONL, outer nuclear layer; OPL, outer plexiform layer; INL, inner nuclear layer; IPL, inner plexiform layer; and GCL, ganglion cell layer.

(C and D) Schematic (C) and example (D) confocal image stack showing expression of AAV2-FLEX-Lin28 in the intact Vglut2-Cre transgenic retina where Lin28 expression is restricted to RGCs and sparse horizontal cells.

(E) Representative confocal image stacks of CTB-labeled RGC axons 2 weeks after optic nerve crush with RGC-restricted expression of Lin28. Asterisks indicate crush site.

(F) Quantification of the extent of RGC axon regeneration in treatment groups restricted to RGCs. Asterisk colors indicate the group that the p value was significant against.

(G) Quantification of RGC survival relative to RGC density observed in intact retinas in treatment groups restricted to RGCs.

Scale bar, 50  $\mu\text{m}$  in (B) and (D), and 200  $\mu\text{m}$  in (E). \*, \*\*, \*\*\*p < 0.05, 0.01, 0.001, respectively.

Because Lin28 expression in RGCs did not induce IGF1 responsiveness, we used a transgenic line that expresses Cre selectively in inhibitory amacrine and horizontal cells (Vgat-Cre) (Vong et al., 2011; Figures 3A and 3B) to target the remaining cellular cohorts that are transduced by AAV2 intravitreal injection

(Figure 2B). Co-injection of AAV2-FLEX-Lin28 and AAV2-IGF1 into Vgat-Cre mice led to robust axon regeneration (Figure 3D), similar to that seen with broad expression of Lin28 (Figures 1B and 1C). Likewise, RGC survival was roughly doubled relative to controls, independent of IGF1 (Figure 3E). Thus, expressing

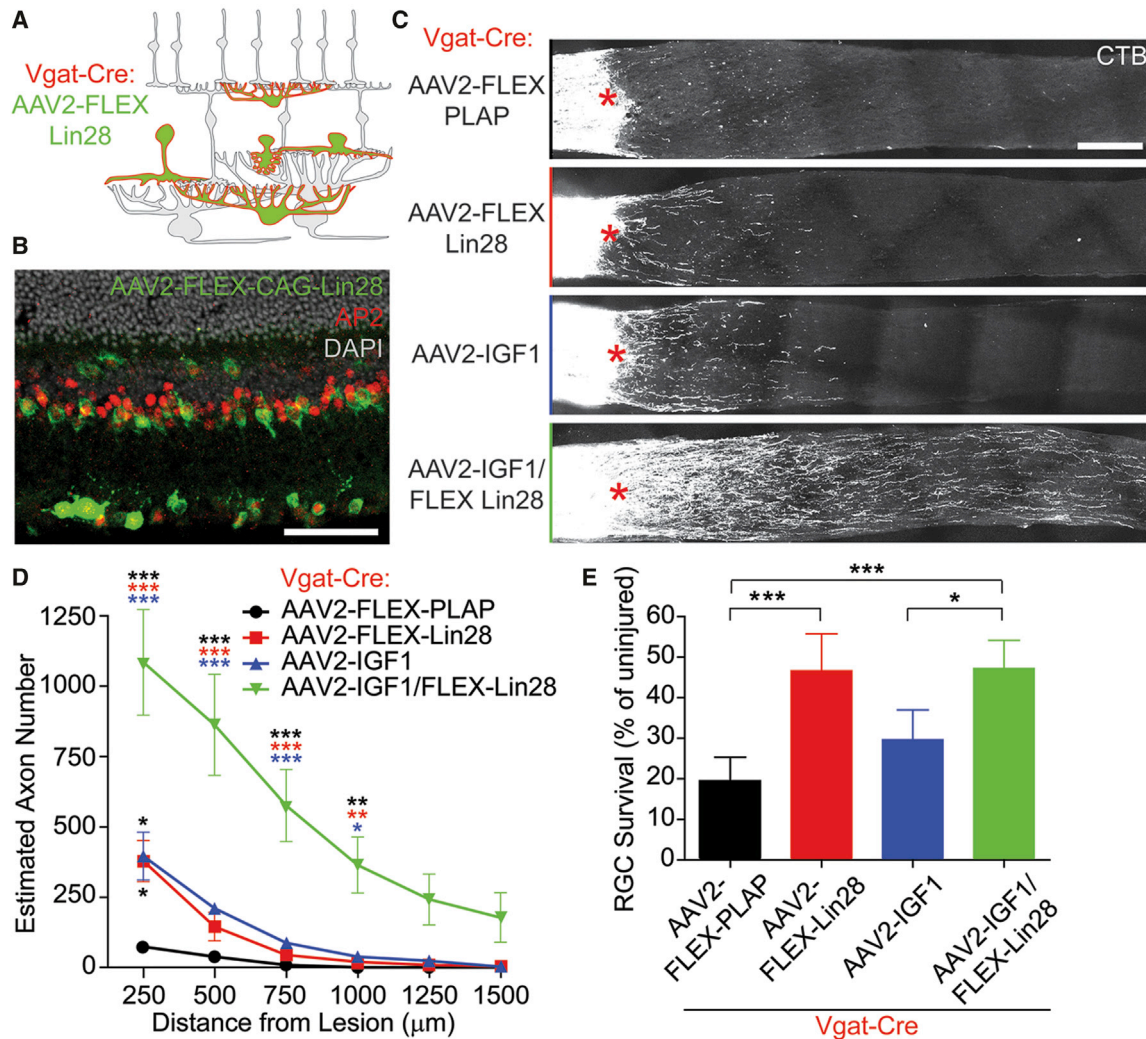


**Figure 3. Lin28 Expression in Inhibitory Neurons Promotes RGC Survival and IGF1-Induced Axonal Regeneration**

(A and B) Schematic (A) and example (B) confocal image stack showing expression of AAV2-FLEX-Lin28 in the intact Vgat-Cre transgenic retina where Lin28 expression is restricted to amacrine and horizontal cells.

(C) Representative confocal image stacks of CTB labeled RGC axons 2 weeks after optic nerve crush with amacrine cell restricted expression of Lin28. Asterisks indicate crush site.

(D) Quantification of the extent of RGC axon regeneration in treatment groups restricted to amacrine cells. Asterisk colors indicate the group that the p value was significant against.

(E) Quantification of RGC survival relative to RGC density observed in intact retinas in treatment groups restricted to amacrine cells. n = 5 mice per group.

Scale bar, 50 µm in (B), and 200 µm in (C). \*, \*\*, \*\*\*p < 0.05, 0.01, 0.001, respectively. See also Figure S2.

Lin28 selectively in inhibitory neurons presynaptic to RGCs, but not RGCs themselves, promoted a robust regenerative response to IGF1 treatment along with IGF1-independent RGC survival.

Even though fewer horizontal cells than amacrine cells are transduced by AAV2 injection, and horizontal cells do not make direct contact with RGCs, we tested their possible contribution to RGC survival and regeneration. Therefore, we used Cx57-Cre transgenic mice, in which Cre expression is limited to horizontal cells (Hirano et al., 2016). Co-injection of AAV2-FLEX-Lin28 and AAV2-IGF1 into Cx57-Cre mice did not significantly increase RGC axon regeneration or survival relative to the minimal regeneration observed with AAV2-IGF1 alone (Fig-

ure S2). Thus, it is likely that the robust neuronal survival and IGF1-dependent axon regeneration observed in Vgat-Cre mice were mainly due to effects on amacrine cells.

#### Optic Nerve Crush Leads to Amacrine Cell Hyperactivation

As Lin28 can reprogram cell metabolism (Shyh-Chang et al., 2013; Zhu et al., 2011) and has been shown to induce modest axon regeneration on its own (Wang et al., 2018), non-cell-autonomous effects on growth-factor responsiveness came as a surprise. RGC activity is reduced after axotomy (Stutzki et al., 2014), but it is unknown whether this is a cell-intrinsic response or

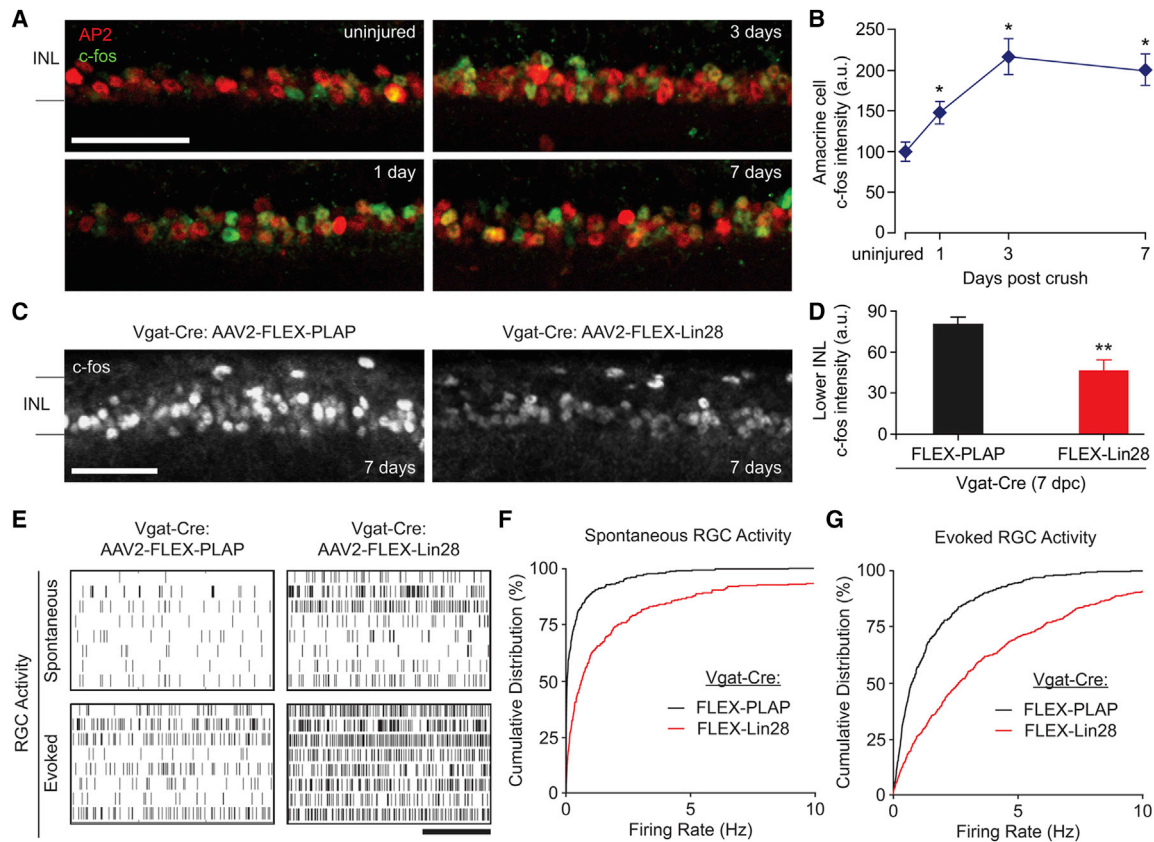


**Figure 4. RGC Axotomy Induced Hyperactivation of Amacrine Cells Is Inhibited by Lin28 Expression**

(A) Confocal image stacks of the INL where AP2-positive amacrine cells (red) are co-labeled with the activity marker *c-fos* (green) at indicated time points after optic nerve crush in untreated mice.  
 (B) Quantification of *c-fos* immunostaining intensity in amacrine cells over time after optic nerve crush.  $n = 6$  mice at least 880 cells per group.  
 (C) Confocal images of *c-fos* expression in the INL of retinas expressing PLAP control (left) or Lin28 in amacrine cells (right) 1 week after optic nerve crush.  
 (D) Quantification of *c-fos* immunostaining intensity of cells in the lower INL from the samples exemplified in (C).  $n = 3$  mice per group.  
 (E) Spike trains from RGC $\alpha$  exemplars recorded in dark-adapted wholemount retinas using a 128-channel multielectrode array following PLAP control or Lin28 expression in amacrine cells at 6 days after optic nerve crush. Spontaneous activity is presented on the upper plots and light-evoked responses to a white noise stimulus on the lower plots. Each row represents activity of a single RGC and each line an action potential.  
 (F and G) Cumulative distribution functions for firing rate of full population of RGCs exemplified in (E) during spontaneous activity (F) and light-evoked activity (G) for PLAP ( $n = 5$  mice, 108 cells) or Lin28 ( $n = 6$  mice, 175 cells) expressing conditions.  
 Scale bar, 50  $\mu\text{m}$  in (A) and (C), and 5 s in (E). \*, \*\* $p < 0.05$ , 0.01, respectively. See also [Figures S3 and S4](#).

resultant to changes in presynaptic activity. Thus, we explored whether optic nerve injury might impact amacrine cell neuronal activity by monitoring expression of an immediate early gene, *c-fos*, which is an established surrogate for neuronal activity (Sheng and Greenberg, 1990) that has been used in the retina to label active neurons for more than two decades (Yoshida et al., 1993; Hanzlicek et al., 2004). In intact mice that were dark adapted, expression of *c-fos* in amacrine cells was relatively low (Figure 4A). However, beginning 24 h after injury, *c-fos* expression in amacrine cells was significantly upregulated, and remained so for at least 1 week (Figures 4A and 4B). While *c-fos* upregulation after injury was primarily seen in amacrine cells, other cells in the inner nuclear layer were also *c-fos* positive although RGCs and photoreceptors remained primarily negative. Vgat-Cre-dependent Lin28 overexpression significantly reduced the injury-induced expression of *c-fos* in the lower inner

nuclear layer where amacrine cells make up the vast majority of neurons (Figures 4C and 4D). Thus, perhaps by homeostatic mechanisms, amacrine cells appear to become hyperactive in response to the injury of RGC axons, and this hyperactivity is reduced by selective Lin28 expression in amacrine cells.

### Blocking Amacrine Cell Synaptic Inhibition Promotes RGC Survival and IGF1-Dependent Regeneration

Because Lin28 is a factor used to induce pluripotency cells in differentiated cells (Wu et al., 2009; Yu et al., 2007), a possibility is that it reverts amacrine cells to an immature state, reducing their activity and ultimately diminishing inhibitory tone onto RGCs. To examine how Lin28 might lead to reductions in amacrine cell electrical activity, we examined mRNA levels of a set of neuronal genes 3 weeks after injection of AAV2-FLEX-Lin28/GFP into Vgat-Cre mice against AAV2-FLEX-GFP-only controls.

Isolated GFP-positive cells were collected by FACs sorting and mRNA purified for ddPCR analysis of the following genes: GABRA1, GABRB3, GRIK1, KCNE2, and KCNH6. All mRNA transcripts were downregulated in Lin28-expressing amacrine cells, some significantly so (Figure S4). As such, we postulate that amacrine cell hyperactivity was suppressed in part by a loss of neuronal character.

Reduced amacrine cell inhibition would lead to more activity in RGCs. As such, we compared RGC electrical activity in control (AAV2-FLEX-PLAP in Vgat-Cre mice) and Lin28-treated (AAV2-FLEX-Lin28 in Vgat-Cre mice), injured retinas using multielectrode array recordings of retinal wholemounts. To do this, freshly dissected dark-adapted retinas were subjected to extracellular action potential recordings with 252-electrode arrays, which mainly record RGC-derived electrical signals (Pearson and Kerschensteiner, 2015). We analyzed both spontaneous activity before light exposure and visual stimulation-evoked responses to a white noise stimulus of constant field luminance. In Vgat-Cre retinas with prior optic nerve injury, Lin28 expression in amacrine cells significantly increased spontaneous RGC activity relative to PLAP controls ( $0.59 \pm 0.11$  Hz in PLAP versus  $3.08 \pm 0.29$  Hz in Lin28,  $p < 0.001$ , Figures 4E and 4F). We also observed higher RGC firing rates during light stimulation ( $1.72 \pm 0.20$  Hz in PLAP versus  $5.32 \pm 0.41$  Hz in Lin28,  $p < 0.001$ , Figures 4E, 4G, S4J, and S4K). Breakdown of RGC subtypes into ON, OFF, and ON-OFF showed that all three subtypes of RGCs fired significantly more with Lin28 expression in amacrine cells (Figure S4A–S4C). In spite of this increase in activity, spatiotemporal-receptive fields of RGCs, as constructed from spike-triggered averages of white noise, were not significantly changed in Lin28-treated retinas, and latency to spike following optimal stimulation was also not changed (Figures S3D–S3I). Together, these results suggest that after optic nerve crush, amacrine cells suppress RGC activity, and this hyperinhibition can be reversed by Lin28 expression in amacrine cells.

Because Lin28-mediated RGC regeneration appeared to act by increasing RGC activity through disinhibition, we next asked if RGC activity itself was a necessary component for the Lin28-mediated regenerative response. To do this, we silenced RGCs by selectively expressing the inward-rectifying-channel Kir2.1 and examined whether Lin28 expression was still able to promote IGF1-elicited axon regeneration (Vglut2-Cre mice treated with AAV2-CAG-IGF1/Lin28 to induce regeneration and AAV2-FLEX-Kir2.1 to silence only RGCs; Figure 5A). We found that Kir2.1 expression specifically in RGCs completely abolished the regeneration phenotypes induced by non-selective Lin28 and IGF1 co-expression (Figures 1B, 1C, 5B, and 5C). Overall, these results support a model by which amacrine cell hyperactivity after optic nerve crush suppresses RGCs, preventing their response to growth factors. Amacrine cell treatment with Lin28 reverses this hyperinhibition, and in turn RGC activity is increased along with subsequent survival and IGF1 responsiveness.

To demonstrate that amacrine cell activity modulation itself allows for IGF1 responsiveness, we directly reduced amacrine cell activity by expressing Kir2.1 in amacrine cells (AAV-FLEX-Kir2.1 into Vgat-Cre mice) and examined RGC regeneration when paired with AAV2-IGF1. With AAV2-FLEX-Kir2.1 alone,

we did not observe significant long-distance optic nerve regeneration. In contrast, the combination of AAV2-IGF1 and AAV2-FLEX-Kir2.1 led to robust axon regeneration (Figures 5D–5F). Moreover, inhibition of amacrine cell activity, either alone or in combination with IGF1, significantly increased RGC cell survival (Figure 5G). Thus, silencing amacrine cells, which also led to significantly more spontaneous RGC activity after injury ( $0.59 \pm 0.11$  Hz in PLAP versus  $0.93 \pm 0.20$  Hz Kir2.1; 108 cells, 5 mice, and Kir2.1, 63 cells, 5 mice, respectively;  $p < 0.05$ ), was sufficient to allow for IGF1-independent RGC survival and IGF1-dependent axon regeneration after injury. While these alterations in activity might seem modest, similar reductions in firing have been previously implicated in homeostatic changes in the CNS (Burrone et al., 2002).

The results above suggested that reducing presynaptic inhibition onto RGCs results in elevated RGC responsiveness to IGF1. To demonstrate that this was indeed the result of reduced inhibitory neurotransmitter signaling, we used a cocktail of drugs to block inhibitory neurotransmitter receptors present on RGC dendrites and bipolar cell axon terminals. Inhibitory signals onto RGC dendrites are primarily mediated by GABA-A and glycine receptors (Grünert, 2000; Tauck et al., 1988), which we blocked with bicuculline and strychnine, respectively. Further, amacrine cells form inhibitory synapses onto bipolar cell axon terminals, which are mainly mediated by glycine and GABA-C receptors (Grünert, 2000; Lukaszewicz et al., 1994; Suzuki et al., 1990; Vaquero and de la Villa, 1999) that can be blocked by 4-imidazoleacetic acid. Thus, a drug cocktail consisting of bicuculline, strychnine, and 4-imidazoleacetic acid was injected, with or without IGF1 protein, every 3 days for 2 weeks after crush (Figure S5A). Although controls demonstrated some spontaneous regeneration, likely due to increased inflammation caused by repeated intraocular injections, the antagonist cocktail alone did not enhance long-distance optic nerve regeneration compared to vehicle controls but did significantly increase RGC survival (Figure S5). Furthermore, axonal regeneration induced by combining the inhibitory receptor antagonist cocktail with IGF1 was significantly greater than either treatment alone (Figures S5B–S5E). Thus, after RGC axotomy, synaptic inhibition mediated by amacrine cells prevents RGC growth factor responsiveness. Importantly, blocking such inhibition by both genetic and pharmacological means was able to restore RGC responses to IGF1, enabling IGF1-induced axon regeneration.

### IGF1R Is Enriched in Healthy RGC Primary Cilia and Is Lost after Injury

Next, we explored the mechanism by which amacrine cell activity affected IGF1 responsiveness of RGCs. First, we examined the expression of IGF1 receptor (IGF1R) protein by immunofluorescence with an anti-IGF1R antibody characterized previously in the CNS (Hollis et al., 2009; Liu et al., 2017). IGF1R immunoreactivity was localized to puncta throughout the thickness of all retinal layers and could be localized to multiple cell types (not shown). Strikingly, on RGC somata, IGF1R signal was concentrated in what appear to be primary cilia (Figures 6A–6C). This localization was verified by demonstrating that IGF1R immunoreactivity was adjacent to and contiguous with pericentrin (Figure 6B), a marker of the ciliary rootlet (Jurczyk et al., 2004).

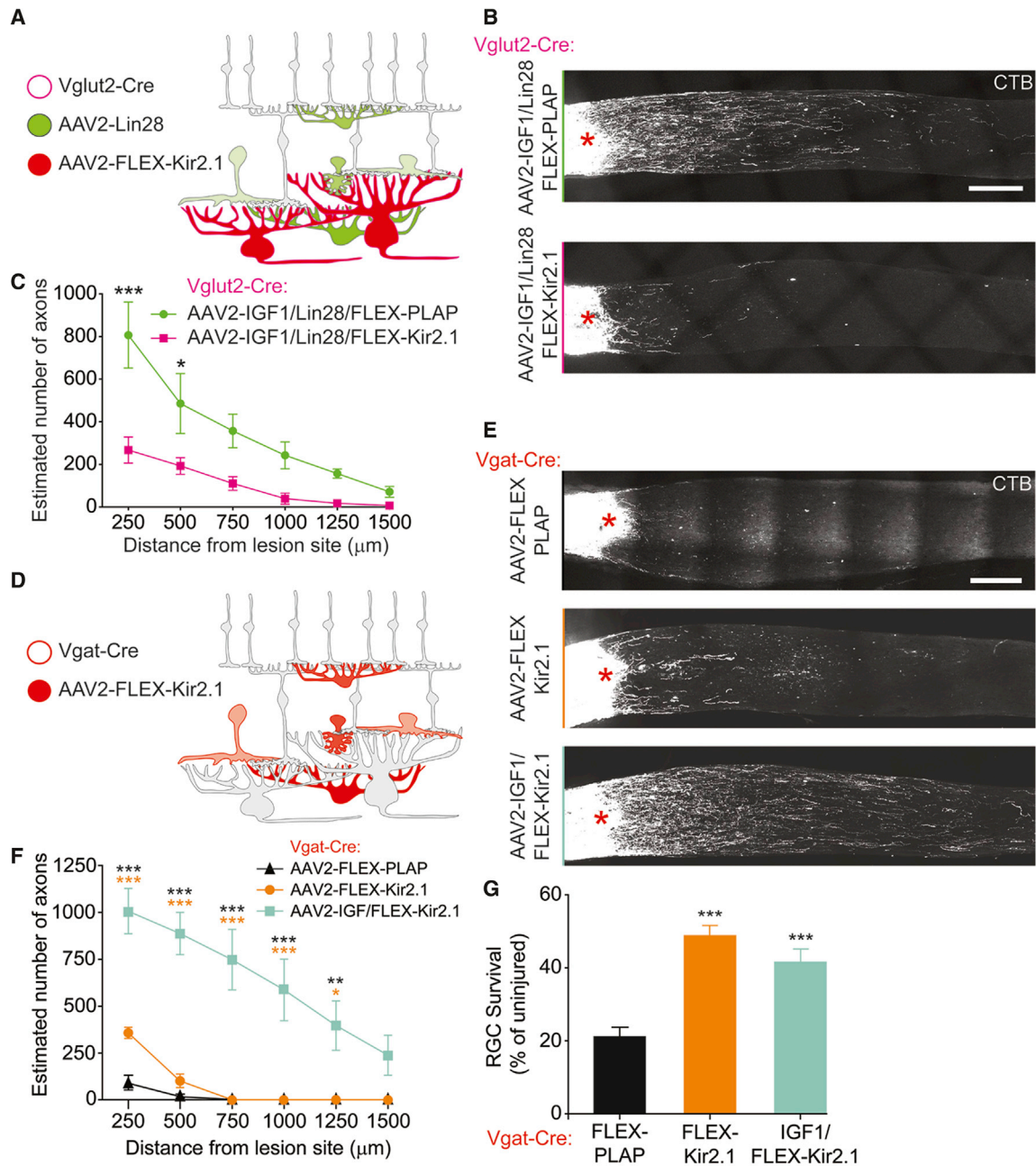


**Figure 5. RGC Activity Is Required for and Amacrine-Cell Hyperinhibition Prevents Lin28- and IGF1-Combinatorial Axon Regeneration**

(A) Schematic of gene expression used to drive regeneration by widespread delivery of AAV2-IGF1/Lin28 (green), along with RGC specific activity silencing via AAV2-FLEX-Kir2.1 (red) injection into Vglut2-Cre (magenta outline) transgenic mice.

(B) Representative confocal image stacks of optic nerve cryosections showing regenerated RGC axons labeled by CTB intraocular injection 2 weeks after crush in control and treatment conditions.

(C) Quantification of the extent of RGC axon regeneration in treatment groups.  $n = 5$  mice per group. Scale bar, 200  $\mu\text{m}$ . \*\*\* $p < 0.001$ .

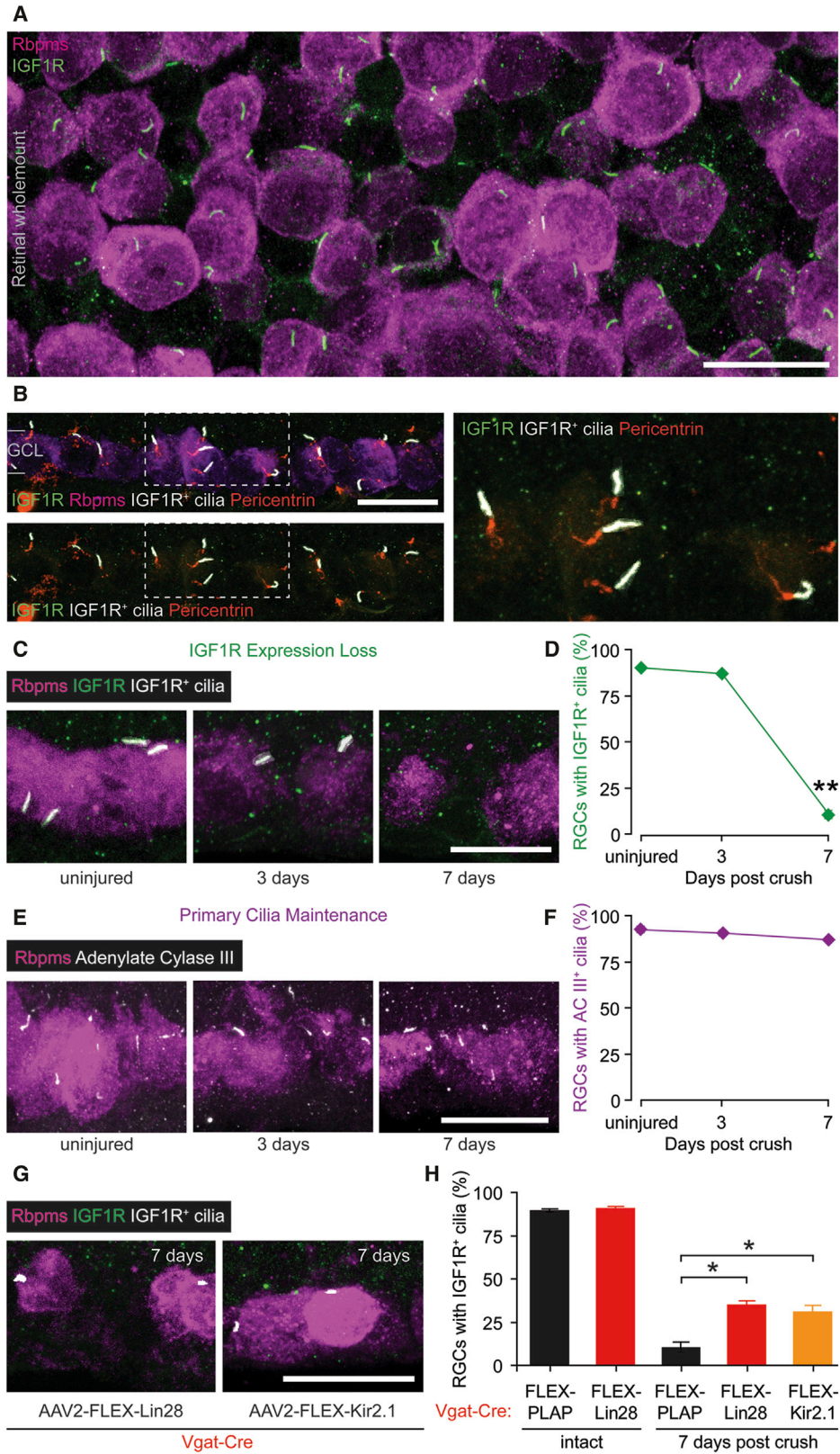
(D) Schematic of gene expression used to silence amacrine cells via AAV2-FLEX-Kir2.1 (red) injection into Vgat-Cre (red outline) transgenic mice.

(E) Representative confocal image stacks of CTB-labeled RGC axons 2 weeks after optic nerve crush with amacrine cell restricted expression of the inhibitory channel Kir2.1 with and without AAV2-IGF1.

(F) Quantification of the extent of axon regeneration following Kir2.1-mediated amacrine cell silencing. Asterisk colors indicate the group that the  $p$  value was significant against.

(G) Quantification of RGC survival following Kir2.1-mediated amacrine cell silencing.  $n = 4-7$  mice per group.

Scale bar, 200  $\mu\text{m}$ . \*, \*\*, \*\*\* $p < 0.05, 0.01, 0.001$ , respectively. See also [Figure S5](#).



(legend on next page)

Antibody specificity was confirmed by absence of cilia staining in a Cre-dependent IGF1R knockout mouse (Figure S6A). From wholemount samples (Figure 6A), it appeared that most, if not all, RGCs have IGF1R immunoreactivity enriched in their cilia, whereas other retinal cells with this feature are rare. In cross sections,  $90.2\% \pm 0.1\%$  of RGCs ( $n = 470$  RGCs, 7 mice) possess single primary cilia with detectable IGF1R signals (Figures 6B and 6C), likely because cryosections contain fragments of RGCs that are missing cilia altogether but stain positive for Rbpms.

Despite the documented role of primary cilia as a signaling center during development (Guemez-Gamboa et al., 2014; Hilgendorf et al., 2016), their role in mature neurons has not been well characterized (Siljee et al., 2018). Examining the expression of IGF1R in RGC cilia after axotomy, we found that by 7 days after optic nerve crush, IGF1R immunoreactivity in RGC cilia was mostly lost (Figures 6C and 6D). This was not due to a loss of cilia in RGCs, as the cilia marker adenylate cyclase III (Bishop et al., 2007) continued to label RGC cilia at this time point (Figures 6E and 6F), although cilia were somewhat shortened in response to injury ( $2.26 \pm 0.05 \mu\text{m}$ ,  $1.67 \pm 0.05 \mu\text{m}$  and  $1.41 \pm 0.04 \mu\text{m}$  in uninjured, 3- and 7-day post crush, respectively). Loss of IGF1R from primary cilia was also not due to suppression of activity in RGCs alone as injection of AAV2-FLEX-Kir2.1 into Vglut2-Cre mice to silence RGCs without injury did not alter IGF1R localization (Figure S6B). Importantly, when Lin28 or Kir2.1 was expressed specifically in amacrine cells, significantly more RGCs maintained IGF1R expression in their cilia (Figures 6G and 6H). Thus, diminishing amacrine cell activity maintained detectable IGF1R expression in the primary cilia of a portion of surviving RGCs.

Because Lin28 promoted BDNF-mediated axon regeneration, we also examined whether BDNF signaling might involve primary cilia localization of the receptor TrkB, but although it localized to photoreceptor inner segments, we did not notice ciliary localization in RGCs (Figure S6C). Taken together with the smaller combinatorial effects of Lin28 and BDNF, we believe the increased regeneration might be due to additive effects.

### Regenerating RGCs Maintain IGF1R in Their Primary Cilia

To distinguish between regenerating and surviving RGCs, we labeled RGCs possessing long-distance regenerating axons with a retrograde tracer, 3 kDa dextran conjugated to biotin, which

was applied to a freshly severed optic nerve stump approximately 1.5 mm distal to the original crush (Figures 7A and 7B). While such labeling efficiently tagged the clear majority of RGCs in the intact retina, tracing after optic nerve crush did not label RGCs in non-regenerating control retinas (not shown). Backtracing in Vgat-Cre mice that were treated with AAV2-FLEX-Lin28 and AAV2-IGF1, 4 weeks after optic nerve crush, led to labeling almost exclusively in Rbpms-positive RGCs (Figures 7C–7E). Importantly, most of these labeled RGCs had IGF1R immunoreactive cilia (Figures 7C and 7F) and were positive for pS6 (Figures 7D and 7F), indicating activation of the mTOR pathway that is downstream of IGF1R signaling. Thus, our results suggest the localization of IGF1R in the primary cilia of adult RGCs represents a key mechanism for their regenerative competency. Decreasing injury induced hyperactivity of amacrine cells via Lin28 or Kir2.1 overexpression maintains IGF1R expression in some RGC primary cilia and ultimately allows them to respond to growth factor treatments and mount a regenerative response.

To examine the RGC subtype specificity of this response, we also immunostained backtraced samples for the alpha-RGC marker osteopontin-1 (OPN1) and found that a majority of regenerating RGCs were alpha-RGCs (Figures 7E and 7F), similar to other regenerative strategies stimulating IGF signaling (Duan et al., 2015). Taken together with the fact that roughly one-third of amacrine cells upregulated *c-fos* after optic nerve crush (Figure 4A) and some amacrine cells subtypes as a whole did not upregulate *c-fos* (Figure S7), we believe that there is likely an aspect of circuit specificity underlying the regenerative mechanisms resultant from amacrine cell inhibition.

### Loss of Primary Cilia Reduces Lin28-Mediated Regeneration

To test the requirement of IGF1R enrichment in cilia, we conditionally knocked out the critical cilia trafficking protein intraflagellar transport protein 88 (IFT88), a transport protein of the primary cilia essential for its formation and maintenance (Haycraft et al., 2007). This manipulation has been previously demonstrated to remove cilia from most examined adult neurons in the hypothalamus within 10 days of the onset of tamoxifen-induced Cre expression (Berbari et al., 2013). Thus, we injected AAV2-Lin28 and AAV2-IGF1 into IFT88-floxed mice along with AAV2-Cre to induce the knockout of IFT88 or AAV2-PLAP as a control (Figure 7G). IFT88 knockout had no effect on axon regeneration in untreated samples (Figures 7H and 7I) and no effect on RGC

**Figure 6. Injury-Induced Loss of IGF1R Enrichment from RGC Primary Cilia Is Prevented by Lin28 or Kir2.1 Expression in Amacrine Cells**

- (A) Confocal image stack of the GCL from a retinal wholemount immunostained for IGF1R (green) and Rbpms (magenta).  
(B) Confocal image stack confirming localization of IGF1R to RGC primary cilia. RGCs were immunolabeled for Rbpms and basal bodies with pericentrin antibodies (red). The lower image is the same as the upper image with the Rbpms signal removed. The image to the right is a zoom in of the boxed region. Ciliary localized IGF1R is pseudocolored in grayscale for clarity.  
(C) Confocal image stacks of IGF1R expression after injury in Rbpms-labeled RGCs.  
(D) Quantification of RGCs with maintained cilia localized IGF1R at indicated time points after lesion.  $n = 4-6$  mice, at least 120 cells per group.  
(E) Confocal image stacks of adenylate cyclase III (grayscale) labeled cilia in Rbpms-labeled RGCs after injury showing that cilia are not lost in axotomized RGCs.  
(F) Quantification of RGCs with adenylate cyclase III at indicated time points after lesion.  $n = 4-6$  mice, at least 120 cells per group.  
(G) Representative confocal image stacks showing that some RGCs maintain ciliary expression of IGF1R at 7 days post injury when amacrine cells express either Lin28 or Kir2.1.  
(H) Quantification of RGCs with maintained IGF1R expression in cilia for indicated conditions.  $n = 4-6$  mice, at least 80 cells per groups.  
Scale bars, 20  $\mu\text{m}$ . \* $p < 0.05$ , \*\* $p < 0.01$ . See also Figure S6.

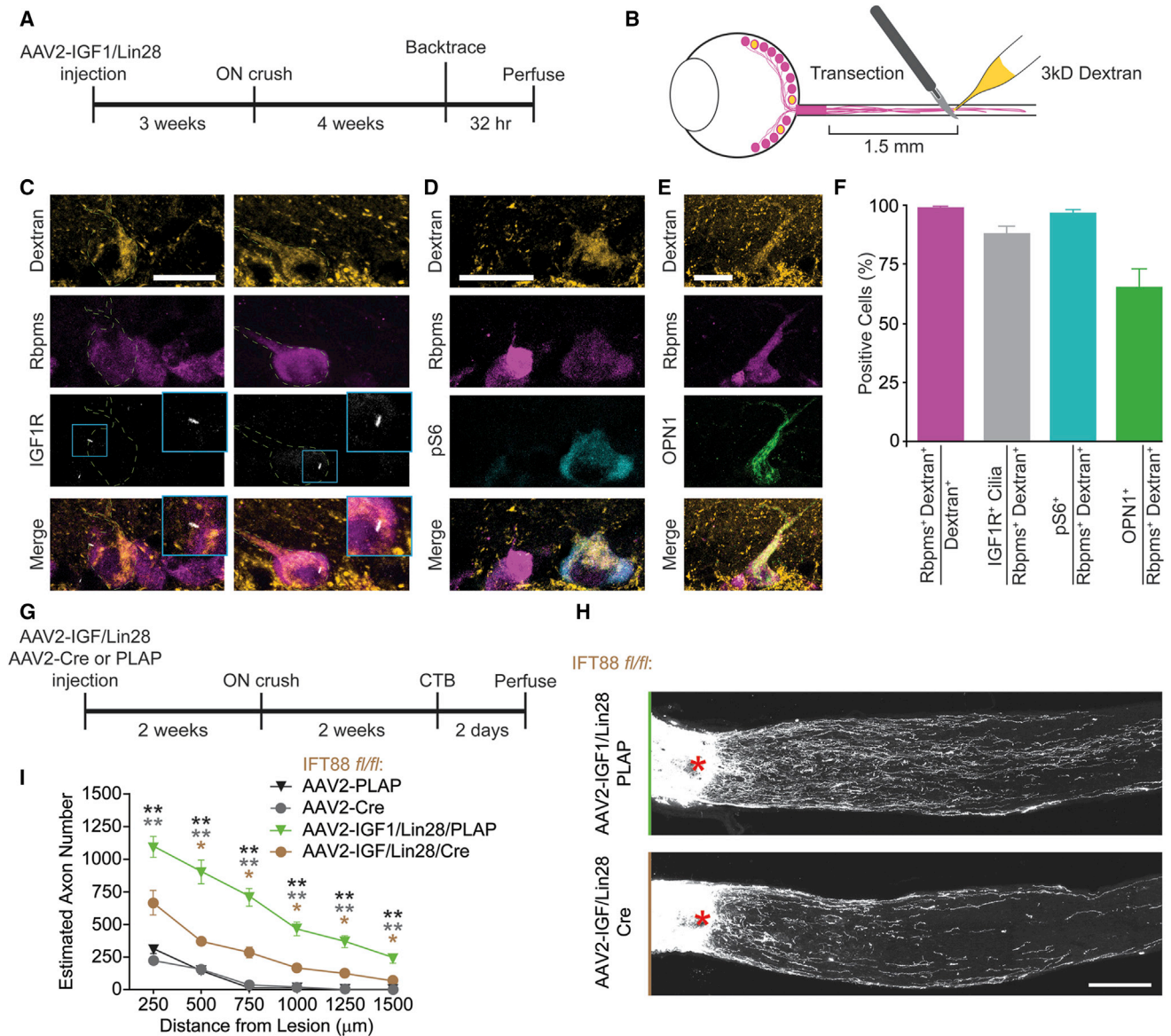


**Figure 7. Regenerating RGCs Maintain IGF1R Expression in Their Primary Cilia**

(A and B) Time course (A) and schematic (B) of backtracing experiments to label cell bodies of regenerated RGCs.

(C) Example confocal image stacks of dextran (yellow) backtraced RGCs labeled with Rbpms (magenta) that maintain expression of IGF1R (grayscale) in their cilia.

(D) Example confocal image stack of dextran backtraced RGC labeled with Rbpms that upregulate phosphorylated S6 (cyan) expression.

(E) Example confocal image stack of dextran backtraced RGC labeled with the alpha-RGC marker OPN1 (green).

(F) Quantification of the rates for which dextran-positive cells were found positive for Rbpms (magenta), dextran and Rbpms double positive cells were found with IGF1R immunoreactive cilia (gray) and were positive for pS6 (cyan) or OPN1 (green) expression (cyan) (n = 5 mice, 350 cells).

(G) Time course of experiments removing primary cilia mediated by IFT88-inducible knockout.

(H) Representative confocal image stacks of optic nerve cryosections showing regenerated RGC axons labeled by CTB intraocular injection 2 weeks after crush in regeneration and cilia knockout conditions.

(I) Quantification of the extent of RGC axon regeneration in treatment groups. n = 4 mice per group.

Scale bar, 20 μm in (C) and (D), and 200 μm in (G). \*p < 0.05, \*\*p < 0.01. See also Figure S7.

survival in either untreated (24.0% ± 0.3% versus 24.1% ± 1.7% in AAV2-PLAP and AAV2-Cre, respectively) or treated (41.6% ± 3.4% versus 40.4% ± 3.2% AAV2-PLAP/IGF/Lin28 versus AAV2-Cre/IGF/Lin28, respectively) conditions. However,

although mice with IFT88 knockout induction still demonstrated moderate regeneration, significantly reduced numbers of regenerating axons were detected in mice with IFT88 deletion relative to regenerating controls (Figures 7H and 7I). A partial effect of

cilia removal is not entirely surprising given that Lin28 itself demonstrated a modest amount of regeneration without IGF1 (Figures 1B and 1C), IGF1R located on RGCs away from the primary cilia can likely still mediate some growth factor response (Zhu et al., 2009), and in our hands AAV2-Cre-mediated inducible knockout of IFT88 only led to a partial loss of primary cilia and corresponding IGF1R enriched cilia in RGCs ( $35.4\% \pm 4.1\%$  and  $44.1\% \pm 3.5\%$  reductions, respectively). Thus, our results suggest that in RGCs primary cilia play an important role for mediating regenerative responses to IGF1.

## DISCUSSION

While available studies have been focused on intrinsic pathways regulating axon-growth ability, our results reveal a mechanism that limits neuronal-regenerative ability in a non-cell-autonomous manner. We found that axotomy triggers a set of homeostatic alterations in the local network that repress the growth potential of injured neurons. This increase in inhibitory synaptic tone onto RGCs following their axotomy ultimately represents a circuit-level brake preventing RGC axon regeneration, by diminishing their responses to growth factors. Further, the homeostatic changes in injured RGCs that are prevented by amacrine cell silencing also play a role in RGC survival independent of growth-factor signaling. Although the amount of regeneration we observed by potentiating IGF1 signaling with amacrine cell silencing was similar to that seen with OPN1-mediated potentiation (Duan et al., 2015), amacrine cell silencing alone doubled the survival of axotomized RGCs (Figure 5G), whereas OPN1-mediated IGF1 potentiation did not enhance RGC survival. Thus, we suspect that while OPN1 signaling likely only alters responsiveness to IGF1, amacrine cell silencing may induce a range of beneficial effects on RGCs in line with treatments that directly increase RGC electrical activity (Li et al., 2016; Lim et al., 2016). Although such beneficial effects seem that they were most robust for the IGF1 growth-factor family (Figure S1).

Importantly, manipulating the activity of amacrine cells or their synaptic connections with RGCs could represent a powerful strategy to regulate RGC growth-factor signaling competence by enhancing their regenerative ability. Indeed, we have demonstrated that a cocktail of inhibitory receptor blockers, some of which have demonstrated human tolerance (Clark, 1938), can improve RGC survival and growth-factor responsiveness. Different hypotheses have been posited to explain the role of neuronal activity in the control of axonal-growth ability. While several studies have implied a positive role (Goldberg et al., 2002; Li et al., 2016; Lim et al., 2016), a different model holds that the development-dependent transition from axon growth to synaptic transmission regulates the loss of axon growth ability (Cohan and Kater, 1986; Enes et al., 2010; Tedeschi et al., 2016). A possible explanation could be relevant to different innervation patterns of the neurons studied: sensory neurons from dorsal root ganglia that lack presynaptic partners in activity-inhibiting studies (Cohan and Kater, 1986; Enes et al., 2010; Tedeschi et al., 2016), and RGCs that have presynaptic partners for studies where axonal regeneration in response to growth factors is potentiated by activity (Goldberg et al., 2002; Li et al., 2016; Lim et al., 2016).

It is quite unexpected that the growth-factor competence induced by Lin28 expression in the retina was not cell intrinsic. While we were able to reproduce very modest axon regeneration seen with non-restricted AAV2 treatments (Wang et al., 2018) (Figures 1B, 1C, 2C, and 2D), as Lin28 is known to promote IGF signal response (Zhu et al., 2011), we might have expected synergistic effects within RGCs themselves. Indeed, our experiments demonstrate the importance of validating cell-intrinsic responses with cell-type-restricted gene expression. While often overlooked, gene expression mediated by intravitreal delivery of AAV2 has been documented for quite some time (Martin et al., 2002; McKinnon et al., 2002). Other transcription factors known to play a role in neuronal development have been shown to induce RGC axon regeneration using gene expression or knockdown systems that would presumably express in amacrine cells as well as RGCs (Moore et al., 2009; Norsworthy et al., 2017). Thus, it is possible that suppression of amacrine cell injury-induced hyperactivity, similar to Lin28, may underlie some of these observations.

It is striking that IGF1-signaling competence is remarkably dependent on the accumulation of IGF1R in primary cilia of these adult RGCs. Our results suggest that the enrichment of growth factor receptors, and perhaps other signaling molecules, in primary cilia could represent a strategy for amplifying neuronal sensitivity to extracellular growth signals and thus regulate their cellular metabolism and function. Indeed, IGF1R enrichment into primary cilia has been observed over the course of adipocyte differentiation (Zhu et al., 2009). Additionally, recent studies have demonstrated that the receptor for melanocortin-4 (MC4R) is enriched in neuronal primary cilia (Siljee et al., 2018). Interestingly, mutations in genes encoding ciliary proteins such as centrosomal protein 19, ankyrin repeat domain 26, adenylate cyclase 3, and MC4R have been shown to cause obesity in mice and humans (Acs et al., 2015; Shalata et al., 2013), suggesting an important role of primary cilia as signaling antennae that regulate organismal metabolism and obesity. A mirrored role for regulating the cellular metabolic state would indicate that ciliary localization of growth factor signaling components could strongly impact an injured neuron's growth potential (He and Jin, 2016). Taken together, our results identify a circuit-level brake on axon regeneration that develops upstream of RGCs as a result of their axonal injury. Overcoming this presynaptic inhibition allows for CNS neurons to respond to growth factors, via a mechanism that maintains growth-factor-receptor localization to primary cilia, and subsequent axon regeneration.

## STAR★METHODS

Detailed methods are provided in the online version of this paper and include the following:

- KEY RESOURCES TABLE
- CONTACT FOR REAGENT AND RESOURCE SHARING
- EXPERIMENTAL MODEL AND SUBJECT DETAILS
  - Mouse Strains
  - Constructs
  - Antibodies

## ● METHOD DETAILS

- Virus Production
- Surgical Procedures
- Perfusions and Tissue Processing
- Immunostaining
- Microscopy
- Image Analysis
- Multielectrode Array (MEA) Recordings
- Visual Stimulation and Analysis
- FACs Sorting and ddPCR

## ● QUANTITATIVE AND STATISTICAL ANALYSIS

## SUPPLEMENTAL INFORMATION

Supplemental Information can be found online at <https://doi.org/10.1016/j.neuron.2019.04.033>.

## ACKNOWLEDGMENTS

We thank Drs. J. Sanes and S. Hegarty for critical reading of the manuscript. This study was supported by grants from the William Randolph Hearst Foundation (P.R.W.), NEI (to N.C.B.), and Dr. Miriam and Sheldon G. Adelson Medical Research Foundation (to Z.H.). This work was supported in part by Career Scientist Award (14F-RCS-004) from the United States Department of Veterans Affairs. IDDRC and viral cores supported by the NIH (P30 HD018655 and P30 EY012196) were used for this study. D.K. was supported by a grant from the NEI (R01EY027411).

## AUTHOR CONTRIBUTIONS

Y.Z., P.R.W., and C.W. performed regeneration, survival, and all other histological procedures. Y.Z. and P.R.W. performed microscopy and image analysis. A.J. performed backtracing surgeries. P.R.W., A.G., and D.K. performed and analyzed multielectrode array experiments. A.A.H. and N.C.B. provided Cx57-Cre transgenic mice. P.R.W. prepared figures. P.R.W. and Z.H. wrote the manuscript and designed experiments.

## DECLARATION OF INTERESTS

The authors have no competing interests to declare.

Received: October 29, 2018

Revised: March 1, 2019

Accepted: April 23, 2019

Published: May 20, 2019

## REFERENCES

- Acs, P., Bauer, P.O., Mayer, B., Bera, T., Macallister, R., Mezey, E., and Pastan, I. (2015). A novel form of ciliopathy underlies hyperphagia and obesity in *Ankrd26* knockout mice. *Brain Struct. Funct.* **220**, 1511–1528.
- Ambros, V. (1989). A hierarchy of regulatory genes controls a larva-to-adult developmental switch in *C. elegans*. *Cell* **57**, 49–57.
- Ambros, V., and Horvitz, H.R. (1984). Heterochronic mutants of the nematode *Caenorhabditis elegans*. *Science* **226**, 409–416.
- Belin, S., Nawabi, H., Wang, C., Tang, S., Latremoliere, A., Warren, P., Schorle, H., Uncu, C., Woolf, C.J., He, Z., and Steen, J.A. (2015). Injury-induced decline of intrinsic regenerative ability revealed by quantitative proteomics. *Neuron* **86**, 1000–1014.
- Berbari, N.F., Pasek, R.C., Malarkey, E.B., Yazdi, S.M., McNair, A.D., Lewis, W.R., Nagy, T.R., Kesterson, R.A., and Yoder, B.K. (2013). Leptin resistance is a secondary consequence of the obesity in ciliopathy mutant mice. *Proc. Natl. Acad. Sci. USA* **110**, 7796–7801.
- Bishop, G.A., Berbari, N.F., Lewis, J., and Mykytyn, K. (2007). Type III adenylyl cyclase localizes to primary cilia throughout the adult mouse brain. *J. Comp. Neurol.* **505**, 562–571.
- Burrone, J., O'Byrne, M., and Murthy, V.N. (2002). Multiple forms of synaptic plasticity triggered by selective suppression of activity in individual neurons. *Nature* **420**, 414–418.
- Chichilnisky, E.J. (2001). A simple white noise analysis of neuronal light responses. *Network* **12**, 199–213.
- Clark, A.J. (1938). *Applied Pharmacology* (Blakiston's Son and Co. Inc.), pp. 255–259.
- Cohan, C.S., and Kater, S.B. (1986). Suppression of neurite elongation and growth cone motility by electrical activity. *Science* **232**, 1638–1640.
- Duan, X., Qiao, M., Bei, F., Kim, I.J., He, Z., and Sanes, J.R. (2015). Subtype-specific regeneration of retinal ganglion cells following axotomy: effects of osteopontin and mTOR signaling. *Neuron* **85**, 1244–1256.
- Ellis, E.M., Gauvain, G., Sivyer, B., and Murphy, G.J. (2016). Shared and distinct retinal input to the mouse superior colliculus and dorsal lateral geniculate nucleus. *J. Neurophysiol.* **116**, 602–610.
- Enes, J., Langwieser, N., Ruschel, J., Carballosa-Gonzalez, M.M., Klug, A., Traut, M.H., Ylera, B., Tahirovic, S., Hofmann, F., Stein, V., et al. (2010). Electrical activity suppresses axon growth through Ca(v)1.2 channels in adult primary sensory neurons. *Curr. Biol.* **20**, 1154–1164.
- Goldberg, J.L., Espinosa, J.S., Xu, Y., Davidson, N., Kovacs, G.T., and Barres, B.A. (2002). Retinal ganglion cells do not extend axons by default: promotion by neurotrophic signaling and electrical activity. *Neuron* **33**, 689–702.
- Goldstein, B.J. (2002). Insulin resistance as the core defect in type 2 diabetes mellitus. *Am. J. Cardiol.* **90** (5A), 3G–10G.
- Grünert, U. (2000). Distribution of GABA and glycine receptors on bipolar and ganglion cells in the mammalian retina. *Microsc. Res. Tech.* **50**, 130–140.
- Guemez-Gamboa, A., Coufal, N.G., and Gleeson, J.G. (2014). Primary cilia in the developing and mature brain. *Neuron* **82**, 511–521.
- Hanzlicek, B.W., Peachey, N.S., Grimm, C., Hagstrom, S.A., and Ball, S.L. (2004). Probing inner retinal circuits in the rod pathway: a comparison of c-fos activation in mutant mice. *Vis. Neurosci.* **21**, 873–881.
- Haycraft, C.J., Zhang, Q., Song, B., Jackson, W.S., Detloff, P.J., Serra, R., and Yoder, B.K. (2007). Intraflagellar transport is essential for endochondral bone formation. *Development* **134**, 307–316.
- He, Z., and Jin, Y. (2016). Intrinsic control of axon regeneration. *Neuron* **90**, 437–451.
- Hilgendorf, K.I., Johnson, C.T., and Jackson, P.K. (2016). The primary cilium as a cellular receiver: organizing ciliary GPCR signaling. *Curr. Opin. Cell Biol.* **39**, 84–92.
- Hirano, A.A., Liu, X., Boulter, J., Grove, J., Pérez de Sevilla Müller, L., Barnes, S., and Brecha, N.C. (2016). Targeted deletion of vesicular GABA transporter from retinal horizontal cells eliminates feedback modulation of photoreceptor calcium channels. *eNeuro* **3**, 3.
- Hollis, E.R., 2nd, Lu, P., Blesch, A., and Tuszynski, M.H. (2009). IGF-I gene delivery promotes corticospinal neuronal survival but not regeneration after adult CNS injury. *Exp. Neurol.* **215**, 53–59.
- Jurczyk, A., Gromley, A., Redick, S., San Agustin, J., Witman, G., Pazour, G.J., Peters, D.J., and Doxsey, S. (2004). Pericentrin forms a complex with intraflagellar transport proteins and polycystin-2 and is required for primary cilia assembly. *J. Cell Biol.* **166**, 637–643.
- Kerschensteiner, D., and Wong, R.O. (2008). A precisely timed asynchronous pattern of ON and OFF retinal ganglion cell activity during propagation of retinal waves. *Neuron* **58**, 851–858.
- Li, S., Yang, C., Zhang, L., Gao, X., Wang, X., Liu, W., Wang, Y., Jiang, S., Wong, Y.H., Zhang, Y., and Liu, K. (2016). Promoting axon regeneration in the adult CNS by modulation of the melanopsin/GPCR signaling. *Proc. Natl. Acad. Sci. USA* **113**, 1937–1942.

- Lim, J.H., Stafford, B.K., Nguyen, P.L., Lien, B.V., Wang, C., Zukor, K., He, Z., and Huberman, A.D. (2016). Neural activity promotes long-distance, target-specific regeneration of adult retinal axons. *Nat. Neurosci.* *19*, 1073–1084.
- Liu, K., Lu, Y., Lee, J.K., Samara, R., Willenberg, R., Sears-Kraxberger, I., Tedeschi, A., Park, K.K., Jin, D., Cai, B., et al. (2010). PTEN deletion enhances the regenerative ability of adult corticospinal neurons. *Nat. Neurosci.* *13*, 1075–1081.
- Liu, Y., Wang, X., Li, W., Zhang, Q., Li, Y., Zhang, Z., Zhu, J., Chen, B., Williams, P.R., Zhang, Y., et al. (2017). A sensitized IGF1 treatment restores corticospinal axon-dependent functions. *Neuron* *95*, 817–833 e814.
- Lukasiewicz, P.D., Maple, B.R., and Werblin, F.S. (1994). A novel GABA receptor on bipolar cell terminals in the tiger salamander retina. *J. Neurosci.* *14*, 1202–1212.
- Martin, K.R.G., Klein, R.L., and Quigley, H.A. (2002). Gene delivery to the eye using adeno-associated viral vectors. *Methods* *28*, 267–275.
- McKinnon, S.J., Lehman, D.M., Tahzib, N.G., Ransom, N.L., Reitsamer, H.A., Liston, P., LaCasse, E., Li, Q., Korneluk, R.G., and Hauswirth, W.W. (2002). Baculoviral IAP repeat-containing-4 protects optic nerve axons in a rat glaucoma model. *Mol. Ther.* *5*, 780–787.
- Moore, D.L., Blackmore, M.G., Hu, Y., Kaestner, K.H., Bixby, J.L., Lemmon, V.P., and Goldberg, J.L. (2009). KLF family members regulate intrinsic axon regeneration ability. *Science* *326*, 298–301.
- Norsworthy, M., Bie, F., Kawaguchi, R., Wang, Q., Tran, N.M., Li, Y., Brommer, B., Zhang, Y., Wang, C., Sanes, J.R., Coppola, G., and He, Z. (2017). Sox11 expression promotes regeneration of some retinal ganglion cell types but kills others. *Neuron* *94*, 1112–1120.
- Park, K.K., Liu, K., Hu, Y., Smith, P.D., Wang, C., Cai, B., Xu, B., Connolly, L., Kramvis, I., Sahin, M., and He, Z. (2008). Promoting axon regeneration in the adult CNS by modulation of the PTEN/mTOR pathway. *Science* *322*, 963–966.
- Pearson, J.T., and Kerschensteiner, D. (2015). Ambient illumination switches contrast preference of specific retinal processing streams. *J. Neurophysiol.* *114*, 540–550.
- Shalata, A., Ramirez, M.C., Desnick, R.J., Priedigkeit, N., Buettner, C., Lindtner, C., Mahroum, M., Abdul-Ghani, M., Dong, F., Arar, N., et al. (2013). Morbid obesity resulting from inactivation of the ciliary protein CEP19 in humans and mice. *Am. J. Hum. Genet.* *93*, 1061–1071.
- Shen, S., Wiemelt, A.P., McMorris, F.A., and Barres, B.A. (1999). Retinal ganglion cells lose trophic responsiveness after axotomy. *Neuron* *23*, 285–295.
- Sheng, M., and Greenberg, M.E. (1990). The regulation and function of c-fos and other immediate early genes in the nervous system. *Neuron* *4*, 477–485.
- Shyh-Chang, N., Zhu, H., Yvanka de Soysa, T., Shinoda, G., Seligson, M.T., Tsanov, K.M., Nguyen, L., Asara, J.M., Cantley, L.C., and Daley, G.Q. (2013). Lin28 enhances tissue repair by reprogramming cellular metabolism. *Cell* *155*, 778–792.
- Siljee, J.E., Wang, Y., Bernard, A.A., Ersoy, B.A., Zhang, S., Marley, A., Von Zastrow, M., Reiter, J.F., and Vaisse, C. (2018). Subcellular localization of MC4R with ADCY3 at neuronal primary cilia underlies a common pathway for genetic predisposition to obesity. *Nat. Genet.* *50*, 180–185.
- Stutzki, H., Leibig, C., Andreadaki, A., Fischer, D., and Zeck, G. (2014). Inflammatory stimulation preserves physiological properties of retinal ganglion cells after optic nerve injury. *Front. Cell. Neurosci.* *8*, 38.
- Suzuki, S., Tachibana, M., and Kaneko, A. (1990). Effects of glycine and GABA on isolated bipolar cells of the mouse retina. *J. Physiol.* *421*, 645–662.
- Tauck, D.L., Frosch, M.P., and Lipton, S.A. (1988). Characterization of GABA- and glycine-induced currents of solitary rodent retinal ganglion cells in culture. *Neuroscience* *27*, 193–203.
- Tedeschi, A., Dupraz, S., Laskowski, C.J., Xue, J., Ulas, T., Beyer, M., Schultze, J.L., and Bradke, F. (2016). The Calcium Channel Subunit Alpha2delta2 Suppresses Axon Regeneration in the Adult CNS. *Neuron* *92*, 419–434.
- Thoenen, H., and Sendtner, M. (2002). Neurotrophins: from enthusiastic expectations through sobering experiences to rational therapeutic approaches. *Nat Neurosci* *5*, 1046–1050.
- Vaquero, C.F., and de la Villa, P. (1999). Localisation of the GABA(C) receptors at the axon terminal of the rod bipolar cells of the mouse retina. *Neurosci. Res.* *35*, 1–7.
- Vong, L., Ye, C., Yang, Z., Choi, B., Chua, S., Jr., and Lowell, B.B. (2011). Leptin action on GABAergic neurons prevents obesity and reduces inhibitory tone to POMC neurons. *Neuron* *71*, 142–154.
- Wang, X.W., Li, Q., Liu, C.M., Hall, P.A., Jiang, J.J., Katchis, C.D., Kang, S., Dong, B.C., Li, S., and Zhou, F.Q. (2018). Lin28 signaling supports mammalian PNS and CNS axon regeneration. *Cell Rep* *24*, 2540–2552 e2546.
- Wu, D., Hamilton, B., Martin, C., Gao, Y., Ye, M., and Yao, S. (2009). Generation of induced pluripotent stem cells by reprogramming human fibroblasts with the stemgent human TF lentivirus set. *J. Vis. Exp.* *8*, 1553.
- Yoshida, K., Kawamura, K., and Imaki, J. (1993). Differential expression of c-fos mRNA in rat retinal cells: regulation by light/dark cycle. *Neuron* *10*, 1049–1054.
- Yu, J., Vodyanik, M.A., Smuga-Otto, K., Antosiewicz-Bourget, J., Frane, J.L., Tian, S., Nie, J., Jonsdottir, G.A., Ruotti, V., Stewart, R., et al. (2007). Induced pluripotent stem cell lines derived from human somatic cells. *Science* *318*, 1917–1920.
- Zhu, D., Shi, S., Wang, H., and Liao, K. (2009). Growth arrest induces primary-cilium formation and sensitizes IGF-1-receptor signaling during differentiation induction of 3T3-L1 preadipocytes. *J. Cell Sci.* *122*, 2760–2768.
- Zhu, H., Shyh-Chang, N., Segrè, A.V., Shinoda, G., Shah, S.P., Einhorn, W.S., Takeuchi, A., Engreitz, J.M., Hagan, J.P., Kharas, M.G., et al.; DIAGRAM Consortium; MAGIC Investigators (2011). The Lin28/let-7 axis regulates glucose metabolism. *Cell* *147*, 81–94.
- Zukor, K., Belin, S., Wang, C., Keelan, N., Wang, X., and He, Z. (2013). Short hairpin RNA against PTEN enhances regenerative growth of corticospinal tract axons after spinal cord injury. *J. Neurosci.* *33*, 15350–15361.

## STAR★METHODS

### KEY RESOURCES TABLE

REAGENT or RESOURCE	SOURCE	IDENTIFIER
<b>Antibodies</b>		
Rabbit anti-Lin28a	Cell Signaling	AB_2297060
Mouse anti-Lin28a	Cell Signaling	AB_1903976
Guinea pig anti-RBPMS	Raygene	Cat# A008712
Rabbit anti-c-Fos	Cell Signaling	AB_2247211
Rabbit anti-IGF1R	Santa Cruz	AB_671788
Rabbit anti-AP2	Abcam	AB_867683
Mouse anti-AP2	Developmental Studies Hybridoma Bank	AB_2313947
Rabbit anti-TrkB	ThermoFisher	AB_2736725
Goat anti-osteopontin 1	R&D Systems	AB_354791
Goat anti-choline acetyl transferase	Millipore	AB_2079751
Rabbit anti-pericentrin	Biologend	AB_2565440
rabbit anti-adenylate cyclase III	ThermoFisher	AB_2552692
rabbit anti-phospho S6	Cell Signaling	AB_2181035
<b>Chemicals, Peptides, and Recombinant Proteins</b>		
Alexa-conjugated cholera toxin subunit B	Thermo Fisher Scientific	C34776
Bicuculline	Sigma	14340
imidazoleacetic acid	Sigma	219991
Strychnine	Sigma	S0532
recombinant human IGF1	Peptotech	100-11
3 kDa dextran conjugated to biotin and TRITC	Thermo Fisher Scientific	D7162
<b>Critical Commercial Assays</b>		
PicoPure RNA Isolation Kit	ThermoFisher	KIT0204
One-Step RT-ddPCR Advanced Kit for Probes	Bio-RAD	1864021
PrimePCR™ ddPCR™ Expression Probe Assay: Tbp, Mouse	Bio-RAD	dMmuCPE5124759
PrimePCR™ ddPCR™ Expression Probe Assay: Grik1, Mouse	Bio-RAD	dMmuCPE5095450
PrimePCR™ ddPCR™ Expression Probe Assay: Gabra1, Mouse	Bio-RAD	dMmuCPE5118172
PrimePCR™ ddPCR™ Expression Probe Assay: Gabrb3, Mouse	Bio-RAD	dMmuCPE5099818
PrimePCR™ ddPCR™ Expression Probe Assay: Kcnh6, Mouse	Bio-RAD	dMmuCPE5115490
PrimePCR™ ddPCR™ Expression Probe Assay: Kcne2, Mouse	Bio-RAD	dMmuCPE5113084
<b>Experimental Models: Organisms/Strains</b>		
Mouse: C57BL/6	Charles River	Strain code#027
Mouse: Vglut2-ires-Cre	Jackson Labs	IMSR_JAX:028863
Mouse: Vgat-ires-Cre	Jackson Labs	IMSR_JAX:016962
Mouse: Connexin 57-Cre	Nicholas Brecha lab from UCLA	N/A
Mouse: IFT88f/f	Jackson Labs	IMSR_JAX:022409
Mouse: IGF1Rf/f	Jackson Labs	IMSR_JAX:012251
<b>Recombinant DNA</b>		
pAAV-CAG-PLAP	BCH Viral Core	N/A
pAAV-CAG-IGF1	BCH Viral Core	N/A
pAAV-CAG-BDNF	BCH Viral Core	N/A
pAAV-CAG-Lin28a	BCH Viral Core	N/A
pAAV-CAG-NT-3	BCH Viral Core	N/A

(Continued on next page)

### Continued

REAGENT or RESOURCE	SOURCE	IDENTIFIER
pAAV-CAG-FLEX-Lin28a	BCH Viral Core	N/A
pAAV-CAG-FLEX-Kir2.1	BCH Viral Core	N/A
pAAV-CAG-FLEX-GFP	BCH Viral Core	N/A
pAAV-CAG-Cre	BCH Viral Core	N/A
Software and Algorithms		
ImageJ	NIH	RRID: SCR_003070
Prism 7.0	GraphPad Software	RRID: SCR_002798
Plexon Offline Sorter	Plexon Inc.	N/A
MATLAB	Mathworks	N/A
Other		
Ultraview Vox Spinning Disk Confocal Microscope	PerkinElmer	N/A
LSM 710 scanning confocal microscope	Zeiss	N/A
256MEA200/30iR-ITO-gr multielectrode array	Multi Channel Systems	N/A
OLED-XL	eMagin	N/A

### CONTACT FOR REAGENT AND RESOURCE SHARING

Further information and requests for reagent will be addressed by the lead author Philip R. Williams ([prwillia@wustl.edu](mailto:prwillia@wustl.edu)).

### EXPERIMENTAL MODEL AND SUBJECT DETAILS

#### Mouse Strains

All experimental procedures were performed in compliance with animal protocols approved by the IACUC at Boston Children's Hospital and Washington University in St. Louis. Mice aged 3-5 weeks at the start of experiments were used throughout. Male and female mice were used in this study at ratios dependent on litters available and with equal distributions across experiments conducted extemporaneously. C57BL6/J, Vglut2-ires-Cre (028863; Jackson Labs), Vgat-IRES-Cre (016962; Jackson Labs), IFT88fl/fl (022409; Jackson Labs) and IGF1Rfl/fl (mouse lines were obtained from Jackson Laboratories. The connexin 57cre (Cx57-Cre) mouse line was described in ([Hirano et al., 2016](#)).

#### Constructs

The AAV-CAG-PLAP, AAV-CAG-IGF1, and AAV-CAG-BDNF expression vectors were previously reported by our lab ([Liu et al., 2017](#)). The AAV-CAG-Lin28a expression vector was cloned by bioabl using the pAAV-MCS backbone (Stratagene). The AAV-CAG-FLEX-Lin28a and AAV-CAG-FLEX-Kir2.1 P2a tdTomato were cloned by Vigene Sciences Inc. using the pAAV-MCS and #60661 (Addgene) backbones respectively.

#### Antibodies

Primary antibodies used were: Rabbit anti-Lin28 (1:500, Cell signaling, 3978); Mouse antiLin28 (1:500, Cell Signaling, 5930); Guinea pig anti-RBPMS (1:2000, Raygene A008712); Rabbit anti-c-Fos (1:500, Cell Signaling, 2250); Rabbit anti-IGF1R (1:500, Santa Cruz, sc-712), rabbit anti-AP2 (1:200, Abcam, 52222), mouse anti-AP2 (1:50, Developmental Studies Hybridoma Bank, 3B5), rabbit anti-pericentrin (1:500, Biolegend, 923701), rabbit anti-adenylate cyclase III (1:500, Thermofisher, PA5-35382) rabbit anti-phospho S6 (1:100, Cell Signaling, 4857), rabbit anti-TrkB (1:20, Thermofisher, PA5-78405), goat anti-osteopontin 1 (1:400x R&D Systems, AF1433), and goat anti-choline acetyl transferase (1:400x Millipore, AB144P). Secondary antibodies were used from Jackson ImmunoResearch or Life Technologies, raised in either goat or donkey against primary antibody's host species, highly cross adsorbed and conjugated to fluorophores of Alexa Fluor 488, Alexa Fluor 568, or Alex Fluor 647, and used at a 1:400-500 dilution. For microruby amplification, streptavidin conjugated to Alexafluor 568 (1:1000, life Technologies, S11226) was used to amplify against the biotin tag.

### METHOD DETAILS

#### Virus Production

Boston Children's Hospital Viral Core provided AAV virus. AAV serotype 2 were used in our study as following: AAV2-PLAP; AAV2-Lin28; AAV2-IGF1; AAV2-BDNF; AAV2-FlexPLAP; AAV2-Flex-Lin28; AAV2-Flex-Kir2.1; AAV2-Flex-GFP; AAV2-Cre. The titers of all viral preparations were at least  $1.0 \times 10^{13}$  GC/mL.

### Surgical Procedures

For all surgical procedures mice were anaesthetized with ketamine and xylazine and received Buprenorphine as a postoperative analgesic.

### AAV Virus Injections

For intravitreal injections, a pulled-glass micropipette was inserted near peripheral retina behind the ora serrata and deliberately angled to avoid damage to the lens. 2–3  $\mu$ L of AAV were injected intravitreally. When two viruses were injected, viruses were pre-mixed to appropriate concentrations and injected in the same volume.

### Drug Injections

A cocktail of inhibitory neurotransmitter receptors (3.33 mM bicuculline, 6.66 mM 4-imidazoleacetic acid and 0.167 mM strychnine in 17% DMSO; all from Sigma, in sterile saline) in 1  $\mu$ L was injected as described above on the time course indicated in fig. S4. For IGF1 treatment, 1  $\mu$ g of recombinant human IGF1 was added to the combination of drugs, or injected in the vehicle solution.

### Optic Nerve Injury

Three weeks after AAV injection, we performed optic nerve injury as previously described (Park et al., 2008). Briefly, the optic nerve was exposed intraorbitally and crushed with fine forceps (Dumont #5 FST) for 5 s approximately 500  $\mu$ m behind the optic disc. Eye ointment was applied post-operatively to protect the cornea. *Anterograde RGC Labeling*: Two to three days before perfusion, 2  $\mu$ L cholera toxin subunit B (CTB-Alexfluor555, 2  $\mu$ g/ $\mu$ L in sterile PBS, ThermoFisher) was injected intravitreally with a pulled glass micropipette attached to a Hamilton syringe (Hamilton).

### Retrograde RGC Labeling

Retrograde labeling of regenerated RGCs was performed as follows. Four weeks after optic nerve crush, mice were anesthetized and placed in a stereotaxic holder. The crushed optic nerve was exposed using a superior temporal intraorbital approach by drilling through the skull and removing overlying brain tissue. After exposing the optic nerve approximately 1.5 mm distal to the crush site, we cut the nerve with a fine blade delivered 100–300 nL of 5% microruby (3 kDa dextran conjugated to biotin and TRITC; ThermoFisher) solution diluted in sterile PBS was delivered to the stump. We then placed a small piece gelfoam (Fisher Scientific) soaked in 5% microruby on the cut nerve stump. The scalp was sutured and animals recovered on a heating pad until they regained consciousness. Mice were perfused 32 hours after the backtracing surgery.

### Perfusions and Tissue Processing

Animals were given an overdose of anesthesia and transcardiacally perfused with ice cold PBS followed by 4% paraformaldehyde (Sigma). For *c-fos* immunostaining, mice were dark adapted overnight, to limit signal from light evoked activity, given anesthesia under dim room light and perfused under normal room lighting. After perfusion, optic nerves and eye balls were dissected out and post-fixed in 4% PFA overnight at 4°C. Tissues were cryoprotected by sinking in 15% sucrose in PBS for optic nerves and 30% sucrose for eyes. Samples were frozen in Optimal Cutting Temperature compound (Tissue Tek) using a dry ice and ethanol bath, then sectioned at 14  $\mu$ m for optic nerves and 20  $\mu$ m for eyes.

### Immunostaining

Immunostaining was performed with the following protocols. All sections were washed with PBS then blocked in a solution of 3% bovine serum albumin (Sigma) or 10% normal donkey serum (Jackson ImmunoResearch) and 0.1%–0.5% Triton X-100 in PBS for 1 h. Samples were then incubated with primary antibodies diluted in the blocking solution overnight. After being washed three times with PBS, secondary antibodies were applied for 2–3 h at room temperature in blocking solution. After being washed three times, sections were mounted onto glass slides with DAPI-Fluoromount-G (VWR) or Vectashield (Vector Labs).

### Microscopy

An Ultraview Vox Spinning Disk confocal microscope (Perkin Elmer) equipped with a 20X air objective was used to acquire image stacks with a 2- $\mu$ m z spacing and 20% overlap in x-y dimensions of optic nerves to assess axon regeneration and retinas to assess RGC survival. Samples were automatically stitched with Velocity software (Perkin Elmer). For cilia and backtracing experiments, an LSM 710 scanning confocal microscope (Zeiss) equipped with a 20 X air or 63 X oil immersion objective was used to acquire z stacks at 2.0  $\mu$ m thickness or 0.6 – 1.0  $\mu$ m thickness respectively. Brightness and contrast of the images were adjusted and pseudo-colored for presentation. Image capture and processing conditions were kept constant when imaging was used for quantification. For display clarification, in images of IGF1R showing cilia, cilia were hand traced in ImageJ and pseudocolored separately from the rest of IGF1R staining in Figure 4 A, B and D.

### Image Analysis

To measure regenerating RGC axons after optic nerve crush, longitudinal sections of optic nerves were serially collected. Regenerating RGC axons were quantified as described previously (Park et al., 2008). CTB labeled axons were estimated by counting the number of CTB labeled fibers extending indicated distances from the crush site across three sections from each nerve to estimate the number of regenerating axons in a biological sample.

All image analysis of the retina was performed on 20  $\mu$ m thick cryosections. For all analyses, where possible, images were collected at the central third of the retina where RGC transduction rates were highest. Rbpms immunostained samples were used to measure

RGC survival after optic nerve crush. RGC numbers were counted from two montaged 20  $\mu\text{m}$  thick retinal sections per animal (approximately 2500–3000  $\mu\text{m}$  per section) using the cell counter plugin from ImageJ software. In intact retina sections, generally 300 to 400 Rbpm positive cells were counted per section. We calculated the linear density of Rbpm positive cells in the GCL and normalized these counts to a standard control non-injured. We also examined INL thickness, a proxy for amacrine cell survival, in our Lin28 and Kir2.1 amacrine cell expression samples and found no difference between PLAP controls, Lin28 treated or Kir2.1 treated retinas ( $34.0 \pm 0.7$ ,  $35.7 \pm 1.0$  and  $33.6 \pm 0.6$   $\mu\text{m}$  respectively,  $n =$  at least 4 mice per group).

To quantify *c-fos* intensity in amacrine cells, single fields of view from 20 X scanning confocal stacks that were stained with AP-2 and *c-fos* antibodies were analyzed in ImageJ. ROIs circling amacrine cells based on AP2 staining were used to blindly measure the signal intensity in the *c-fos* channel. For Lin28 treated samples, the combination of AP2 and *c-fos* antibodies was not possible, therefore we analyzed *c-fos* intensity in the ‘lower’ inner nuclear layer by generating a large ROI across a maximum intensity projected image that contained the 2 – 3 cell bodies proximal to the inner plexiform layer interface using the DAPI channel as a guide.

To quantify IGF1R and ACIII staining, confocal scanning images acquired with the 63 X oil immersion objective were used to first identify presumptive primary cilia and then those contained within or contiguous with an Rbpm positive (or Rbpm and dextran double positive) cell body in the inner plexiform layer were counted along with Rbpm positive cells lacking cilia. When a confocal color channel was available, pericentrin immunostaining was included to aid in identification of primary cilia.

### Multielectrode Array (MEA) Recordings

Mice were killed in a CO<sub>2</sub> chamber, and retinas were dissected in ice cold mouse artificial cerebrospinal fluid (125 NaCl, 2.5 KCl, 1.25 Na<sub>2</sub>HPO<sub>4</sub>, 2 CaCl<sub>2</sub>, 1 MgCl<sub>2</sub>, 20 Glucose, 26 NaHCO<sub>3</sub>, 0.5 L-Glutamine in mM equilibrated with 95% O<sub>2</sub> 5% CO<sub>2</sub>) under dim red light. We recorded extracellular action potentials on planar 252-electrode arrays (Multi Channel Systems, electrode size: 10  $\mu\text{m}$ , center-center distance: 100  $\mu\text{m}$ ). During recordings, retinas were perfused at 6 – 8 mL/min with warm (33°C) mouse artificial cerebrospinal fluid. We bandpass filtered signals of all electrodes (300 – 3,000 Hz), digitized them (10 kHz), and acquired 3-ms cut-outs whenever signals crossed a threshold set manually for each electrode. We then sorted these waveforms into spike trains representing the activity of individual cells using principal component analysis (Offline Sorter, Plexon). We analyzed the cross-correlation of spike trains to detect when one neuron had been recorded on multiple electrodes. In these cases, only the train with the most spikes was used for further analysis.

### Visual Stimulation and Analysis

We wrote visual stimuli in MATLAB (Mathworks) using the Cogent Graphics toolbox extensions developed by John Romaya at the LON at the Wellcome Department of Imaging Neuroscience, and projected them from an organic light emitting display (OLEDXL, eMagin) through a 20 X 0.5 NA water immersion objective (Olympus) onto the retina. The display output was linearized using custom scripts. In the checkerboard white noise stimulus, the intensity of squares of 50  $\mu\text{m}$  side length was chosen at random from a Gaussian distribution every 33 ms (refresh rate: 30 Hz). The mean stimulus intensity was 1,000 rhodopsin isomerizations / rod / s (1,000 R\*), and the stimulus contrast (SD / mean) 40%. We used a linear – nonlinear cascade model to describe the light responses of RGCs (Chichilnisky, 2001 and Kerschensteiner and Wong, 2008). We calculated the linear part of this model, the spatiotemporal receptive field of the RGC, from its spike-triggered stimulus average (STA). To calculate the nonlinear part of the model, the dependence of the RGC activity on the match between the stimulus and the RGC’s spatiotemporal receptive field, we convolved the stimulus with the STA. The timevarying output of this convolution is called the generator signal. We split the range of generator signals into 25 bins and calculated the average spike rate in these bins to complete the model. Linear and nonlinear parts of the model were estimated in separate parts of the recording. To measure an RGC’s receptive field size, we fit a 2D Gaussian to the spatial profile at the temporal peak of the STA, and calculated the equivalent radius of the ellipse at 1 SD. To measure response timing of an RGC, we calculated the delay of the temporal peak in the STA. We measured the peak response of an RGC as the average firing rate in its highest generator signal bin.

### FACs Sorting and ddPCR

ddPCR was performed in triplicate with 4 retinas combined per sample. FACs sorting was carried out as previously described (Norsworthy et al., 2017). Briefly, Vgat-Cre transgenic mice were deeply anesthetized and decapitated 3 weeks after intraocular injection of either AAV2-FLEX-GFP or AAV2-FLEX-Lin28 and AAV2-FLEX-GFP. Eyeballs were removed and retinas were dissected in chilled Hanks balanced salt solution (HBSS, Life Technologies, 14170-112) with 10 mM HEPES added. 3-4 retinas were pooled per sample into 2 mL of 37°C digestion solution (HBSS with HEPES (Sigma, H3375), 0.032% w/v L-cysteine (Sigma, C7477), 50  $\mu\text{g}/\text{mL}$  DNase (Sigma, D4527), 1U/ $\mu\text{L}$  papain (Worthington, LS003126), filtered through a 0.22  $\mu\text{m}$  filter (Millipore, SCGP00525) before adding 40 U/mL Protector RNase Inhibitor (Roche, 03335399001)). Samples were digested for 4 min at 37°C and then centrifuged at 450Xg for 4 min at 4°C. The supernatant was discarded and cells resuspended in digestion inhibitor (MEM with phenol Red (Life Technologies, 11090-081) containing 1% w/v bovine serum albumin (BSA, Sigma, A2153), 1% w/v trypsin inhibitor from egg white (Sigma, T9253) 50  $\mu\text{g}/\text{mL}$  DNase, filtered through a 0.22  $\mu\text{m}$  filter before adding 20 U/mL Protector RNase Inhibitor) by titrating up and down 8-10 times as needed. Samples were centrifuged for at 350-400Xg for 40 s at 4°C, and the supernatant was saved. Pellets were resuspended as before and this process was repeated until only a minimal pellet remained. The collected cells were filtered through a 40  $\mu\text{m}$  cell strainer (Fisher, 08-771-1), centrifuged for at 450Xg for 10 min at 4°C, the supernatant discarded and the pellet

resuspended in 1–4 mL of DMEM (Life Technologies, 31053-028) containing 0.4% BSA, 5 U/mL Protector RNase and 1  $\mu$ M calcein blue (Sigma, M1255). FACS sorting was performed using a BD FACSAria II Flow Cytometer equipped with a 70  $\mu$ m nozzle using a filter set for DAPI excitation to screen viable calcein blue positive cells and GFP expressing virally infected cells. Samples were sorted directly into Extraction Buffer from the Arcturus PicoPure RNA Isolation Kit (ThermoFisher, KIT0204)

RNA was purified using the Arcturus PicoPure RNA Isolation Kit according to the manufacturers instructions. ddPCR was performed using the One-Step RT-ddPCR Advanced Kit (Bio-RAD, 1864021). ddPCR Expression Probes for *Grik1*, *Gabra1*, *Gabbr3*, *Kcne2* and *Kcne2* (Bio-RAD, dMmuCPE5095450, dMmuCPE5118172, dMmuCPE5099818, dMmuCPE5115490, dMmuCPE5113084) were measured according to the manufacturer's instructions and normalized to levels of *Tbp* (Bio-RAD, dMmuCPE5124759).

### QUANTITATIVE AND STATISTICAL ANALYSIS

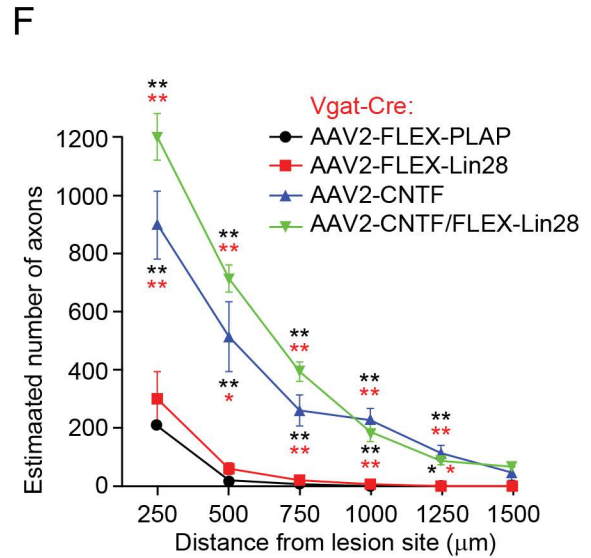
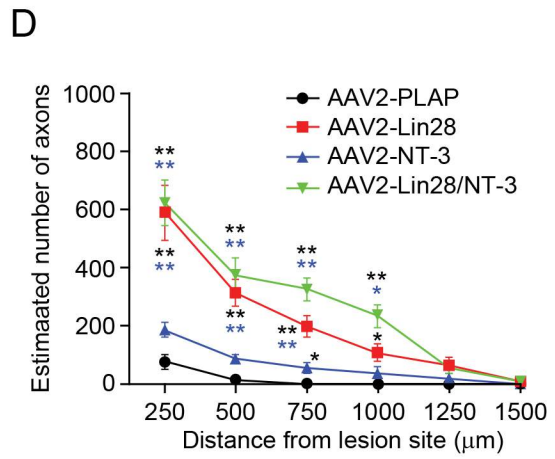
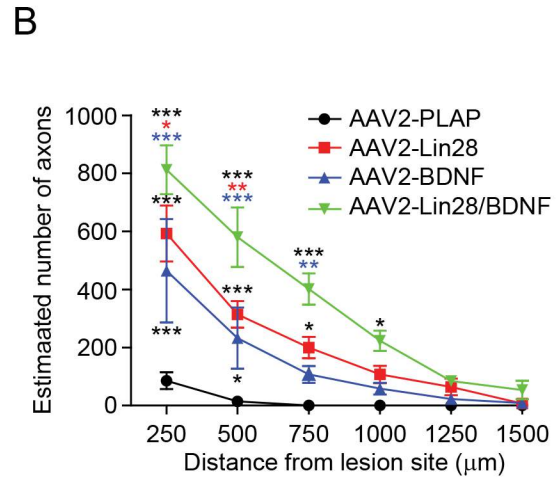
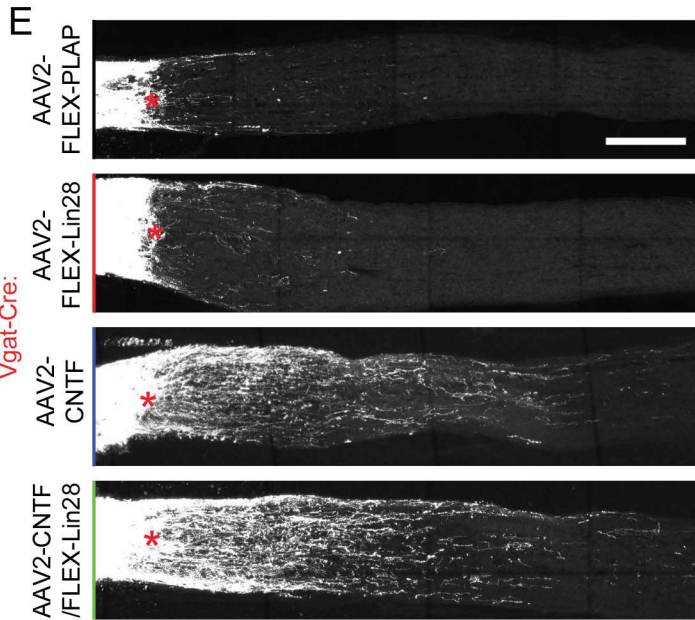
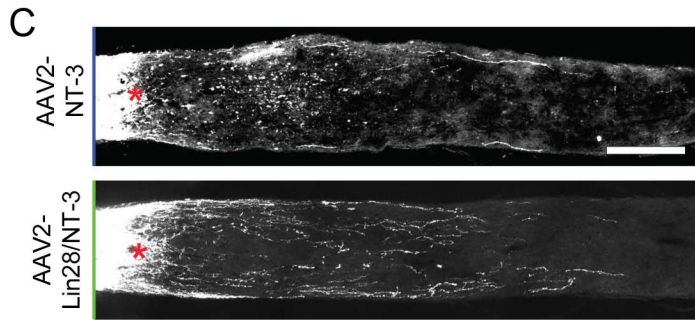
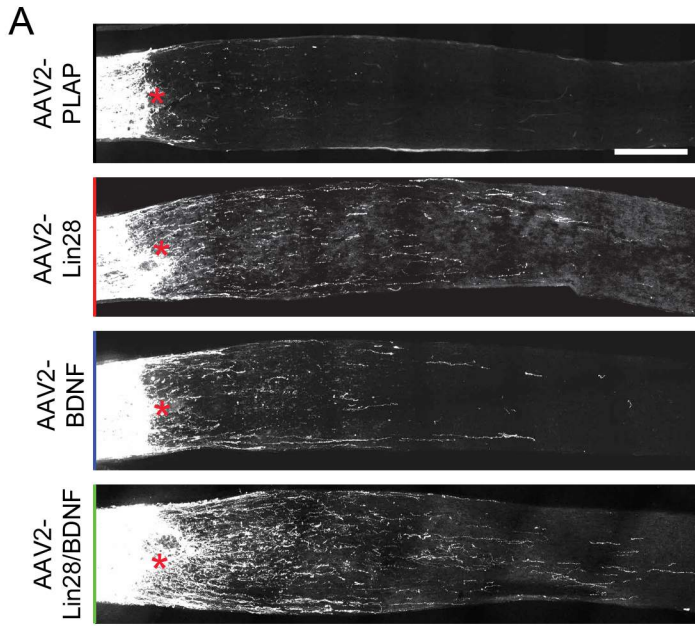
One-way ANOVAs with Bonferroni Correction were performed with PRISM software to examine statistical significance of axon regeneration data. Mann-Whitney U-Test was used for two group comparisons. Error bars represent the SEM.

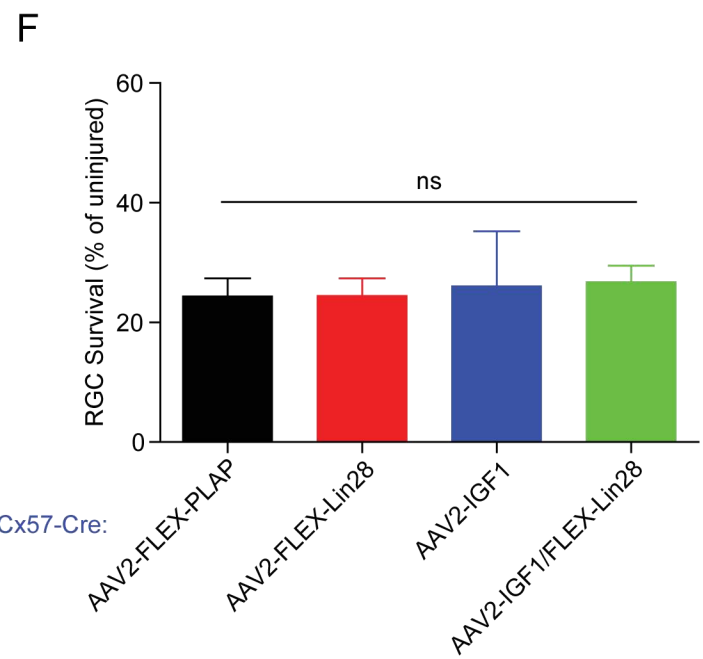
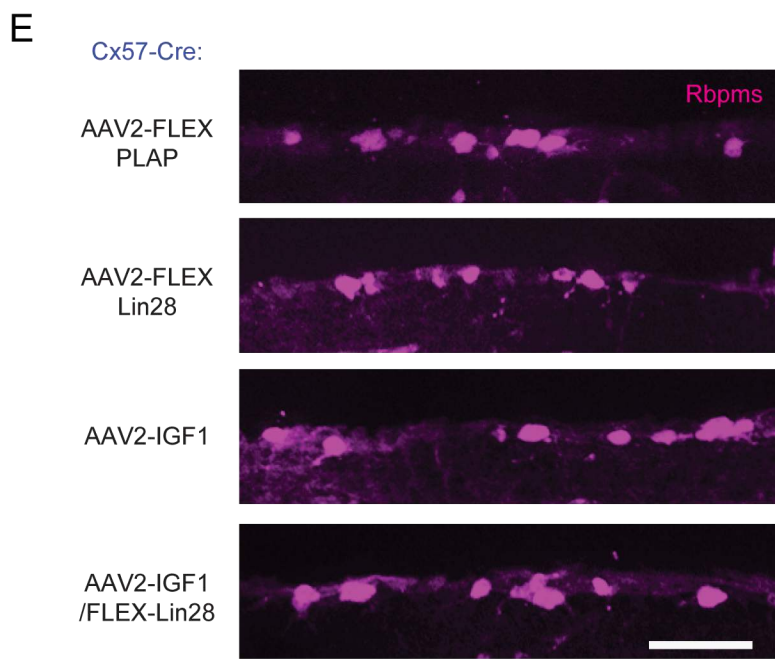
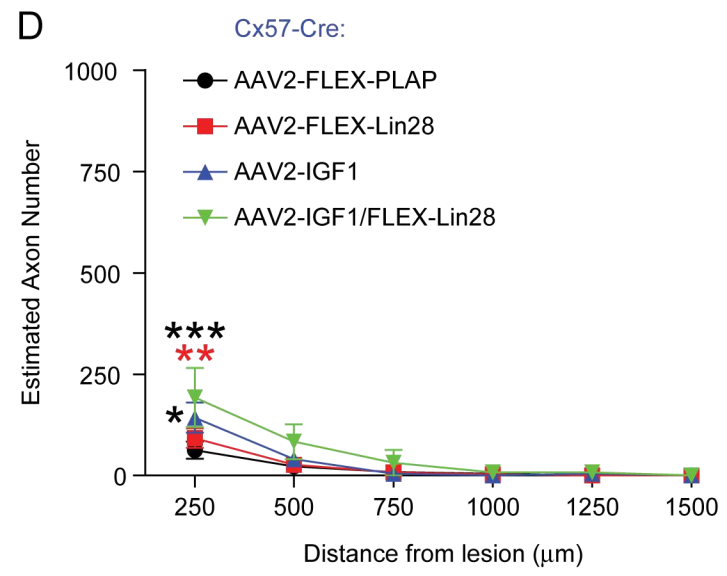
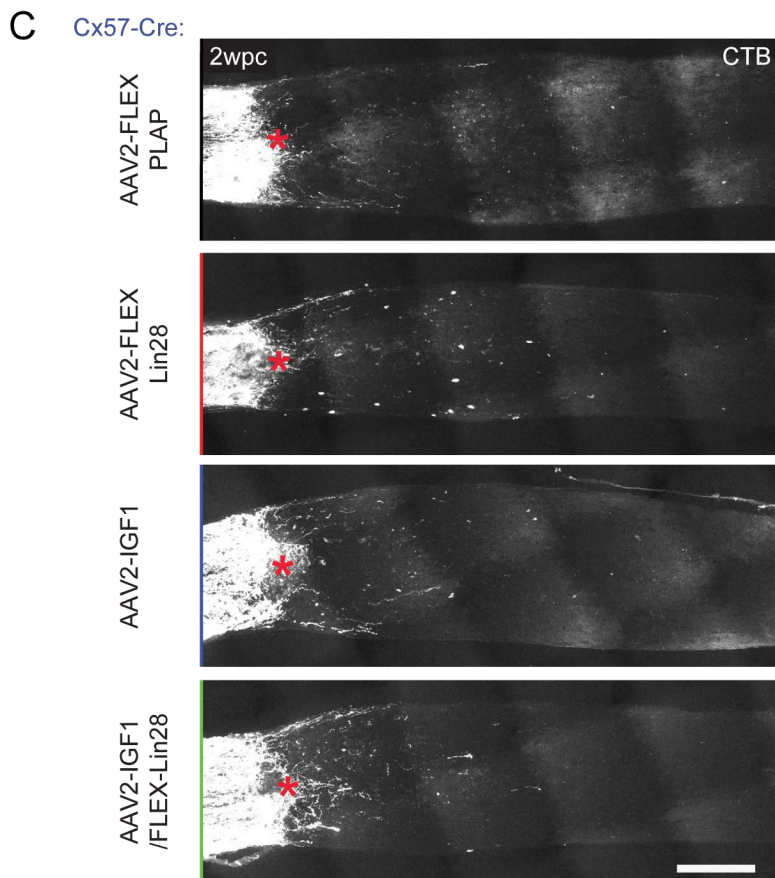
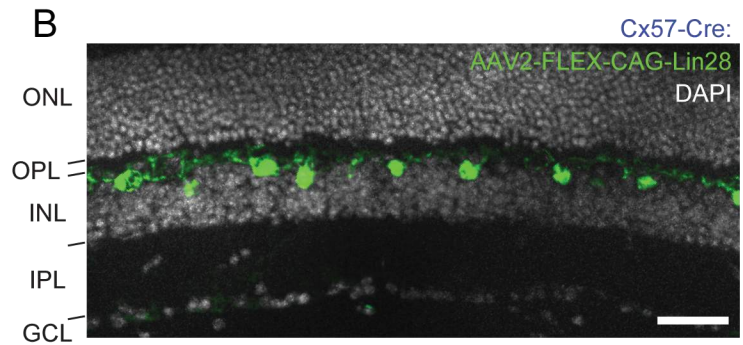
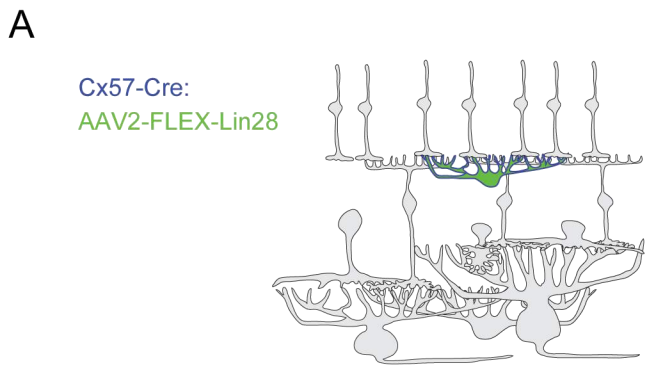
**Neuron, Volume 103**

**Supplemental Information**

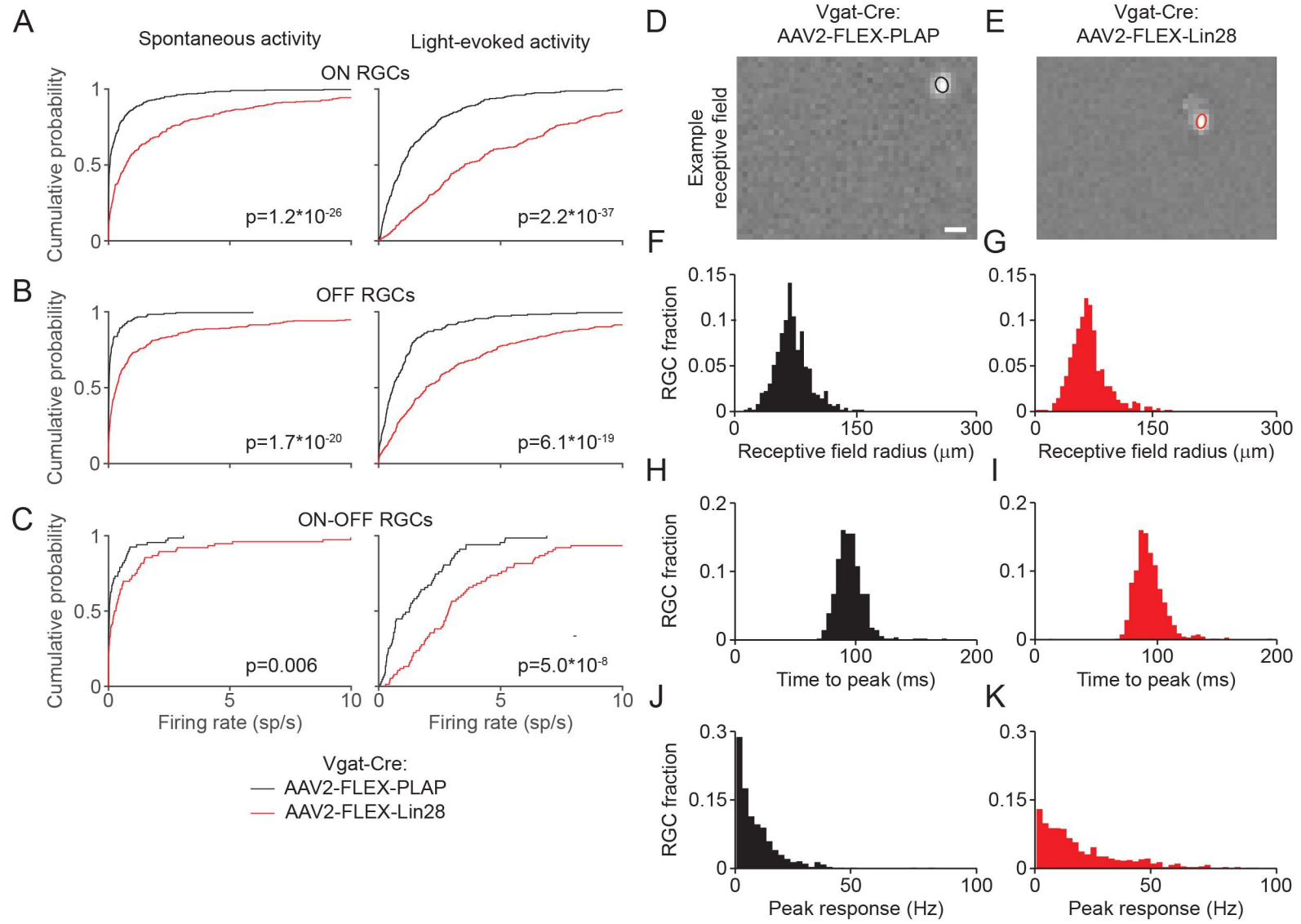
**Elevating Growth Factor Responsiveness and Axon  
Regeneration by Modulating Presynaptic Inputs**

**Yiling Zhang, Philip R. Williams, Anne Jacobi, Chen Wang, Anurag Goel, Arlene A. Hirano, Nicholas C. Brecha, Daniel Kerschensteiner, and Zhigang He**

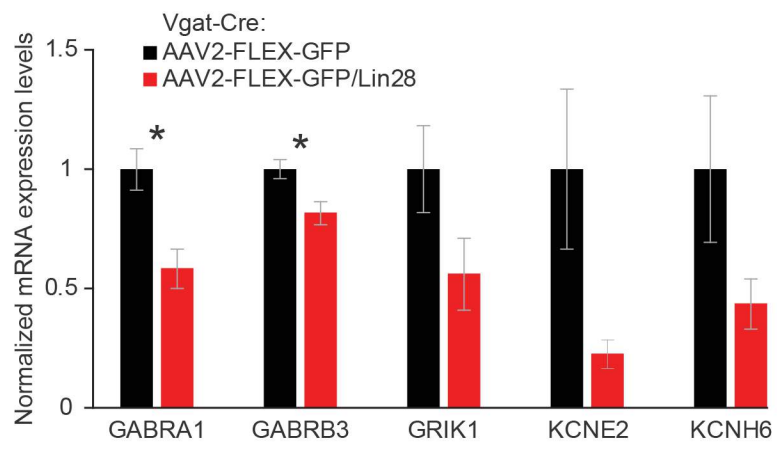


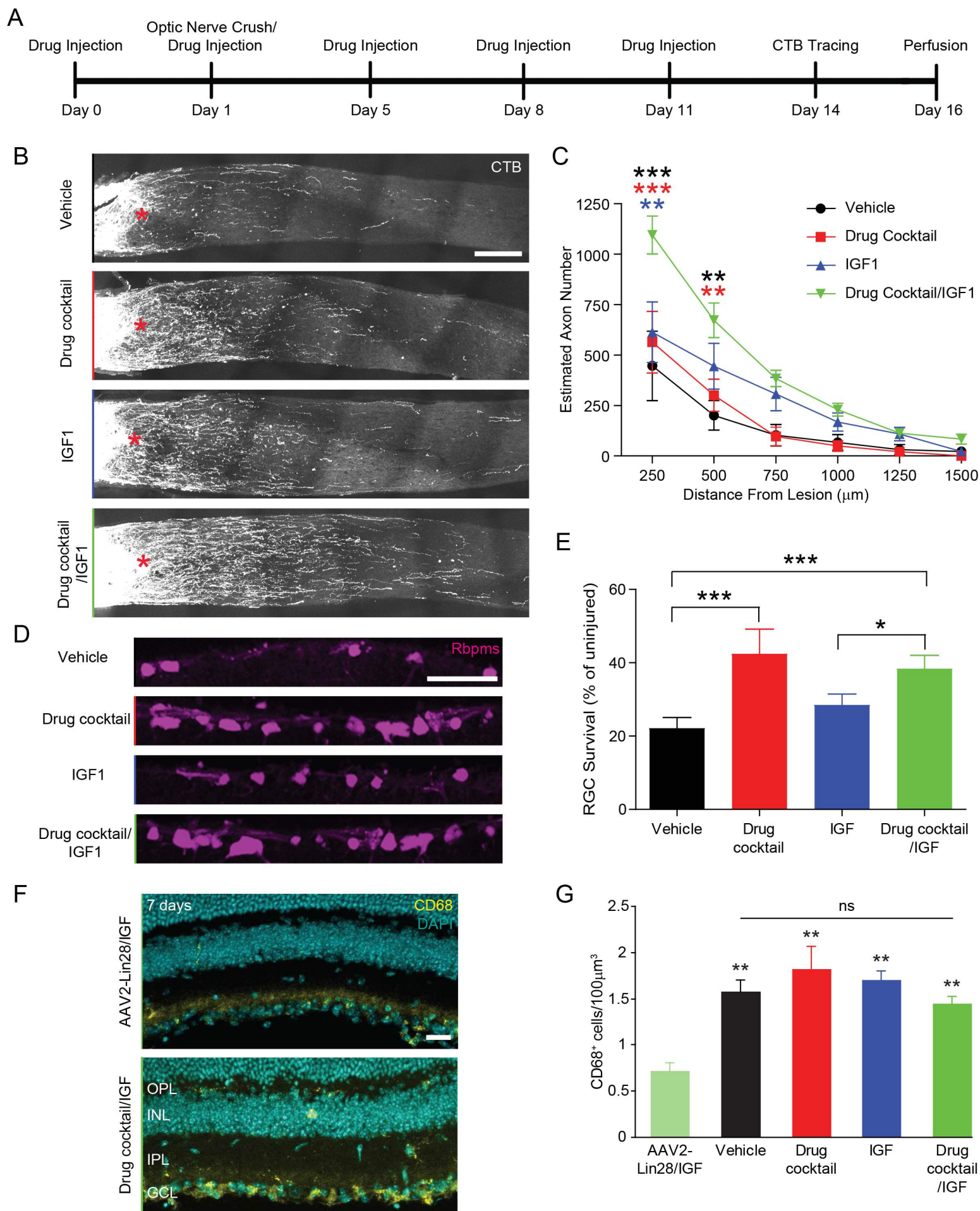


Supplemental Figure 2

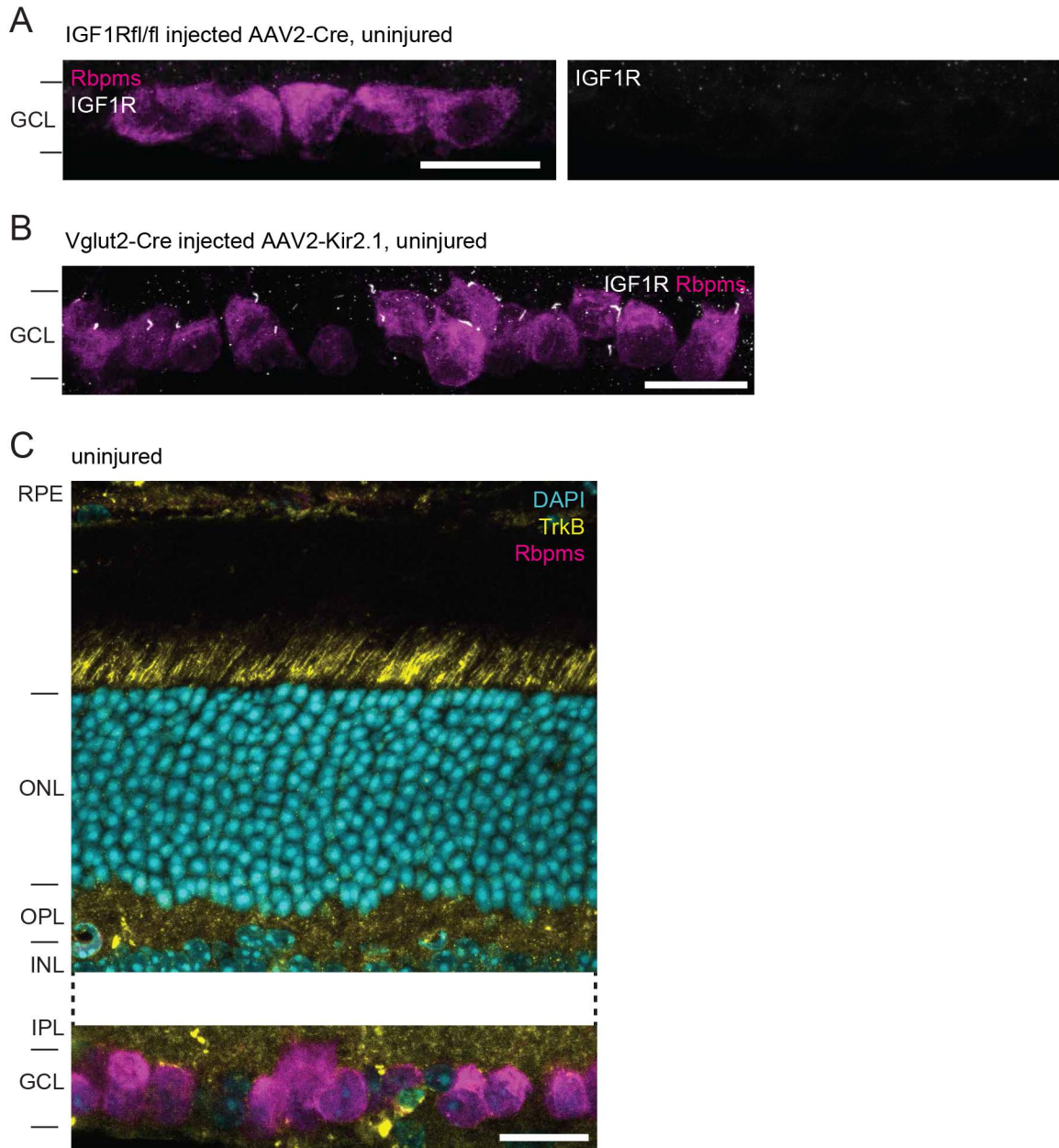


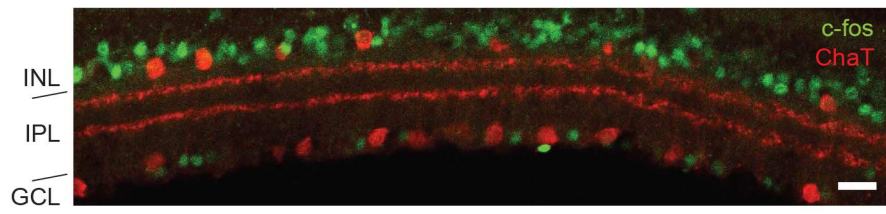
Supplemental Figure 3





Supplemental Figure 5





## SUMMPLEMENTAL FIGURE LEGENDS

**Supplemental Figure 1. Lin28 expression potentiates BDNF but not NT-3 responsiveness, Related to Figure 1.** (A) Representative confocal image stacks of optic nerve cryosections showing regenerated RGC axons labeled by CTB intraocular injection two weeks after crush in control and indicated BDNF treatment conditions. (B) Quantification of the extent of RGC axon regeneration in BDNF treatment groups. Asterisk colors indicate the group that the p value was significant against. n = 4-5 mice per group. (C) Representative confocal image stacks of optic nerve cryosections showing regenerated RGC axons labeled by CTB intraocular injection two weeks after crush in control and indicated NT-3 treatment conditions. (D) Quantification of the extent of RGC axon regeneration in NT-3 treatment groups. Asterisk colors indicate the group that the p value was significant against. n = 4-6 mice per group. (E) Representative confocal image stacks of optic nerve cryosections showing regenerated RGC axons labeled by CTB intraocular injection two weeks after crush in control and indicated Vgat-Cre CNTF treatment conditions. (F) Quantification of the extent of RGC axon regeneration in Vgat-Cre CNTF treatment groups. Asterisk colors indicate the group that the p value was significant against. n = 3-4 mice per group. Scale bars = 200  $\mu$ m. \*, \*\*, \*\*\* p < 0.05, 0.01, 0.001 respectively.

**Supplemental Figure 2. Horizontal cell specific expression of Lin28 does not induce RGC survival or robust IGF1 responsiveness, Related to Figure 3.** (A) Schematic of Cre dependent Lin28 expression in the Cx57-Cre transgenic retina. (B) Example confocal image stack showing expression of AAV2-FLEX-Lin28 in the intact Cx57-Cre transgenic retina where Lin28 (green) expression is restricted to horizontal cells. DAPI is in grayscale. (C) Representative confocal image stacks of CTB labeled RGC axons two weeks after optic nerve crush with horizontal cell restricted expression of Lin28. (D) Quantification of the extent of RGC axon regeneration in treatment groups. Asterisk colors indicate the group that the p value was significant against. (E) Representative confocal image stacks of retinal cross-sections stained with the RGC marker Rbpms. (F) Quantification of RGC survival in treatment groups relative to RGC density observed in intact retinas. n = 3-4 mice per group. Scale bar = 50  $\mu$ m in panels B and E, and 200  $\mu$ m in panel C. \* p < 0.05.

**Supplemental Figure 3. General RGC response properties are not altered by Lin28 expression in amacrine cells, Related to Figure 4.** (A) Cumulative distribution plots of spontaneous (left) and light evoked (right) activity of ON RGCs in retinas with amacrine cells expressing Lin28 (red) or PLAP control (black) 6 days after optic nerve crush. (B) Cumulative

distribution plots of spontaneous (left) and light evoked (right) activity of OFF RGCs in retinas with amacrine cells expressing Lin28 (red) or PLAP control (black) 6 days after optic nerve crush. (C) Cumulative distribution plots of spontaneous (left) and light evoked (right) activity of ON-OFF RGCs in retinas with amacrine cells expressing Lin28 (red) or PLAP control (black) 6 days after optic nerve crush. (D, E) Example receptive fields reproduced from spike triggered averages of RGC responses to white noise stimuli in retinal wholemounts where PLAP (D) and Lin28 (E) are expressed in amacrine cells 6 days after optic nerve crush. (F, G) Distribution of receptive field size by fraction of RGCs in retinas expressing PLAP (F) or Lin28 (G) specifically in amacrine cells. (H, I) Distribution of the time to peak for RGC action potentials generated by light stimulation in retinas expressing PLAP (H) or Lin28 (I) in amacrine. (J, K) Distribution of the proportion of RGCs plotted by peak firing rate between retinas expressing PLAP (J) or Lin28 (K) in amacrine cells. Scale bar = 200  $\mu\text{m}$ .

**Supplemental Figure 4. Altered neuronal transcripts in Lin28 overexpressing amacrine cells, Related to Figure 4.** Expression levels of indicated mRNA measured by ddPCR from FACs sorted amacrine cells three weeks after delivery of AAV2-FLEX-GFP (black) or AAV2-FLEX-Lin28/FLEX-GFP (red) to Vgat-Cre transgenic mice. Measurements were normalized to the housekeeping gene TATA binding protein and then to control samples. n = 3 samples with 4 retinas per sample. \* p < 0.05.

**Supplemental Figure 5. Blockade of inhibitory neurotransmission recapitulates Lin28 or Kir2.1 expression in amacrine cells, Related to Figure 5.** (A) Mice received 1  $\mu\text{l}$  intraocular injections of an inhibitory neurotransmitter receptor blocking cocktail (3.33 mM bicuculline, 6.66 mM I4AA and 0.167 mM strychnine in 17% DMSO) or vehicle control with or without 1  $\mu\text{g}$  of IGF1 recombinant protein according to the schedule indicated. (B) Representative confocal image stacks of CTB labeled RGC axons two weeks after optic nerve crush following drug and/or recombinant IGF1 treatment. (C) Quantification of the extent of RGC axon regeneration in treatment groups. Asterisk colors indicate the group that the p value was significant against. (D) Representative confocal image stacks of retinal cross-sections stained with the RGC marker Rbpms. (E) Quantification of RGC survival in treatment groups relative to RGC density observed in intact retinas. (F) Representative confocal images stacks from retinas of indicated samples stained for CD68 to label activated immune cells and microglia (yellow) and DAPI (cyan). (G) Quantification of the density of CD68<sup>+</sup> cells in retinal sections. n = 4-5 mice per group. Scale bar = 200  $\mu\text{m}$  and 50  $\mu\text{m}$  in panels B and D respectively. \*, \*\*, \*\*\* p < 0.05, 0.01, 0.001 respectively.

**Supplemental Figure 6. IGF1R localization to RGC primary cilia is specific and independent of RGC activity, Related to Figure 6.** (A) Confocal image stack of RGCs labeled with Rbpms (magenta) in an IGF1R<sup>f1/fl</sup> retina injected with AAV2-Cre four months prior to fixation. No ciliary immunostaining of IGF1R (gray) was observed in any RGCs examined (n = 39). (B) Vglut2-Cre mice were treated with AAV2-FLEX-Kir2.1 without injury and examined 4 weeks later. IGF1R immunostaining was not affected. (C) Example confocal stack of uninjured retina labeled for TrkB (yellow) and DAPI (cyan). Scale bar = 20  $\mu$ m.

**Supplemental Figure 7, Related to Figure 7. Not all amacrine cell subtypes upregulate c-fos after optic nerve crush.** Example immunostaining of starburst amacrine cells with choline acetyltransferase (ChAT) antibodies (red) along with c-fos (green) 7 days after optic nerve crush. Few if any starburst amacrine cells were found with high levels of c-fos expression. Scale bar = 20  $\mu$ m.